2. Allen DN, Strauss GP, Donohue B, van Kammen DP (2007) Factor analytic support for social cognition as a separable cognitive domain in schizophrenia. Schizophr Res 93:325–333
3. Anderson SW, Damasio AR, Damasio H (1990) Troubled letters but not numbers. Domain specific cognitive impairments following focal damage in frontal cortex. Brain 113(Pt 3):749–766
4. Arai T, Hasegawa M, Akiyama H, Ikeda K, Nonaka T, Mori H, Mann D, Tsuchiya K, Yoshida M, Hashizume Y, Oda T (2006) TDP-43 is a component of ubiquitin-positive tau-negative inclusions in frontotemporal lobar degeneration and amyotrophic lateral sclerosis. Biochem Biophys Res Commun 351:602–611
5. Basso A, Taborelli A, Vignolo LA (1978) Dissociated disorders of speaking and writing in aphasia. J Neurol Neurosurg Psychiatry 41:556–563
6. Baxter DM, Warrington EK (1986) Ideational agraphia: a single case study. J Neurol Neurosurg Psychiatry 49:369–374
7. Brooks BR, Miller RG, Swash M, Munsat TL (2000) El Escorial revisited: revised criteria for the diagnosis of amyotrophic lateral sclerosis. Amyotroph Lateral Scler Other Motor Neuron Disord 1:293–299
8. Caselli RJ, Windebank AJ, Petersen RC, Komori T, Parisi JE, Okazaki H, Kokmen E, Iverson R, Dinapoli RP, Graff-Radford NR et al (1993) Rapidly progressive aphasic dementia and motor neuron disease. Ann Neurol 33:200–207
9. Cedarbaum JM, Stambler N, Malta E, Fuller C, Hilt D, Thurmond B, Nakanishi A (1999) The ALSFRS-R: a revised ALS functional rating scale that incorporates assessments of respiratory function. BDNF ALS Study Group (Phase III). J Neurol Sci 169:13–21
10. Ferrer I, Roig C, Espino A, Peiro G, Matias Guiu X (1991) Dementia of frontal lobe type and motor neuron disease. A Golgi study of the frontal cortex. J Neurol Neurosurg Psychiatry 54:932–934
11. Heilman K (2003) clinical neuropsychology. Oxford university press, Oxford
12. Ichikawa H, Kawamura M (2010) Language impairment in amyotrophic lateral sclerosis. Brain Nerve 62:435–440
13. Ichikawa H, Koyama S, Ohno H, Ishihara K, Nagumo K, Kawamura M (2008) Writing errors and anosognosia in amyotrophic lateral sclerosis with dementia. Behav Neurol 19:107–116
14. Ichikawa H, Takahashi N, Hieda S, Kawamura M (2010) Bulbar-onset amyotrophic lateral sclerosis (ALS) with isolated agraphia. Rinsho Shinkeigaku 50:81–86
15. Ichikawa H, Takahashi N, Hieda S, Ohno H, Kawamura M (2008) Agraphia in bulbar-onset amyotrophic lateral sclerosis: not merely a consequence of dementia or aphasia. Behav Neurol 20:91–99
16. Kanzaki M, Sato M, Ogawa G, Miyamoto N, Motoyoshi K, Kamakura K, Takeda K (2004) A case of dementia with motor neuron disease associated with agraphia—the omission of kana letters. Rinsho Shinkeigaku 44:673–676
17. Lomen-Hoerth C, Murphy J, Langmore S, Kramer JH, Olney RK, Miller B (2003) Are amyotrophic lateral sclerosis patients cognitively normal? Neurology 60:1094–1097
18. Mackenzie IR, Bigio EH, Ince PG, Geser F, Neumann M, Cairns NJ, Kwong LK, Forman MS, Ravits J, Stewart H, Eisen A, McClusky L, Kretzschmar HA, Monoranu CM, Highley JR, Kirby J, Siddique T, Shaw PJ, Lee VM, Trojanowski JQ (2007) Pathological TDP-43 distinguishes sporadic amyotrophic lateral sclerosis from amyotrophic lateral sclerosis with SOD1 mutations. Ann Neurol 61:427–434
19. Mochizuki H, Ohtomo R (1988) Pure alexia in Japanese and agraphia without alexia in kanji. The ability dissociation between reading and writing in kanji vs. kana. Arch Neurol 45:1157–1159
20. Murphy JM, Henry RG, Langmore S, Kramer JH, Miller BL, Lomen-Hoerth C (2007) Continuum of frontal lobe impairment in amyotrophic lateral sclerosis. Arch Neurol 64:530–534
21. Neary D, Snowden JS, Gustafson L, Passant U, Stuss D, Black S, Freedman M, Kertesz A, Robert PH, Albert M, Boone K, Miller BL, Cummings J, Benson DF (1998) Frontotemporal lobar degeneration: a consensus on clinical diagnostic criteria. Neurology 51:1546–1554
22. Neumann M, Mackenzie IR, Cairns NJ, Boyer PJ, Markesbery WR, Smith CD, Taylor JP, Kretzschmar HA, Kimonis VE, Forman MS (2007) TDP-43 in the ubiquitin pathology of frontotemporal dementia with VCP gene mutations. J Neuropathol Exp Neurol 66:152–157
23. Nishihira Y, Tan CF, Onodera O, Toyoshima Y, Yamada M, Morita T, Nishizawa M, Kakita A, Takahashi H (2008) Sporadic amyotrophic lateral sclerosis: two pathological patterns shown by analysis of distribution of TDP-43-immunoreactive neuronal and glial cytoplasmic inclusions. Acta Neuropathol 116:169–182
24. Otsuki M, Soma Y, Arai T, Otsuka A, Tsuji S (1999) Pure apraxic agraphia with abnormal writing stroke sequences: report of a Japanese patient with a left superior parietal haemorrhage. J Neurol Neurosurg Psychiatry 66:233–237
25. Piquard A, Le Forestier N, Baudoin-Madec V, Delgadillo D, Salachas F, Pradat PF, Derouesne C, Meininger V, Lacomblez L (2006) Neuropsychological changes in patients with primary lateral sclerosis. Amyotroph Lateral Scler 7:150–160
26. Ringholz GM, Appel SH, Bradshaw M, Cooke NA, Mosnik DM, Schulz PE (2005) Prevalence and patterns of cognitive impairment in sporadic ALS. Neurology 65:586–590
27. Sakurai Y, Matsumura K, Iwatsubo T, Momose T (1997) Frontal pure agraphia for kanji or kana: dissociation between morphology and phonology. Neurology 49:946–952
28. Satoh M, Takeda K, Kuzuhara S (2009) Agraphia in intellectually normal Japanese patients with ALS: omission of kana letters. J Neurol 256:1455–1460
29. Seki R, Ishiai S, Koyama Y, Sato S, Seki K (2000) Aphasia and paragraphia of kana letters following infarction in the posterior middle and inferior frontal gyri. Japanese J Neuropsychol 16:127–134
30. Shean G, Meyer J (2009) Symptoms of schizophrenia and social cognition. Psychiatry Res 170:157–160
31. Soma Y, Sugishita M, Kitamura K, Maruyama S, Imanaga H (1989) Lexical agraphia in the Japanese language. Pure agraphia for Kanji due to left poster inferior temporal lesions. Brain 112 ((Pt 6)):1549–1561
32. Strong MJ, Grace GM, Freedman M, Lomen-Hoerth C, Woolley S, Goldstein LH, Murphy J, Shoesmith C, Rosenfeld S, Leigh PN, Bruijn L, Ince PG, Figlewicz D (2009) Consensus criteria for the diagnosis of frontotemporal cognitive and behavioural syndrome in amyotrophic lateral sclerosis. Amyotroph Lateral Scler 10:131–146
33. Tohgi H, Saitoh K, Takahashi S, Takahashi H, Utsugisawa K, Yonezawa H, Hatano K, Sasaki T (1995) Agraphia and acalculia after a left prefrontal (F1, F2) infarction. J Neurol Neurosurg Psychiatry 58:629–632
34. Zago S, Poletti B, Corbo M, Adobbati L, Silani V (2008) Dysgraphia in patients with primary lateral sclerosis: a speech-based rehearsal deficit? Behav Neurol 19:169–175

JOURNAL OF VIROLOGY, June 2010, p. 5947–5957 Vol. 84, No. 12
0022-538X/10/$12.00 doi:10.1128/JVI.02575-09

2A Protease Is Not a Prerequisite for Poliovirus Replication▽†

Hiroko Igarashi,[1] Yasuko Yoshino,[1] Miwako Miyazawa,[2] Hitoshi Horie,[2,3] Seii Ohka,[1]* and Akio Nomoto[1]#

Department of Microbiology, Graduate School of Medicine, The University of Tokyo, 7-3-1 Hongo, Bunkyo-ku, Tokyo 113-0033, Japan[1]; Japan Poliomyelitis Research Institute, Tokyo, Japan[2]; and Department of Microbiology, Faculty of Pharmaceutical Science, Ohu University, Fukushima, Japan[3]

Received 9 December 2009/Accepted 5 April 2010

Poliovirus (PV) $2A^{pro}$ has been considered important for PV replication and is known to be toxic to host cells. A $2A^{pro}$-deficient PV would potentially be less toxic and ideal as a vector. To examine whether $2A^{pro}$ is needed to form progeny virus, a full-length cDNA of dicistronic (*dc*) PV with (pOME) or without (pOMEΔ2A) $2A^{pro}$ was constructed in the strain PV1(M)OM. RNAs of both pOME and pOMEΔ2A were capable of forming progeny viruses, called OME and OMEΔ2A, respectively. In their ability to induce a cytopathic effect (CPE), the strains ranked as OMEΔ2A < OME ≒ PV1(M)OM. These results suggest that $2A^{pro}$ is not essential for full-length *dc* PV to form progeny virus and that it contributes to the efficient viral replication and/or induction of a CPE. To clarify whether $2A^{pro}$ is essential for P1-null (lacking the entire coding sequence for capsid proteins) PV, the RNA replication activity of P1-null PV (pOMΔP1) or P1-null PV without $2A^{pro}$ (pOMΔP1Δ2A) or without both $2A^{pro}$ and 2B (pOMΔP1Δ2AΔ2B) was examined. The RNAs of pOMΔP1 and pOMΔP1Δ2A could replicate and form progeny viruses under a *trans* supply of P1 protein, whereas the RNA of pOMΔP1Δ2AΔ2B could not. These results suggest that $2A^{pro}$ is not needed for the replication of P1-null PV, although it is important for PV RNA replication and inducing a CPE. To know whether a $2A^{pro}$-deficient PV can be used as a vector, a P1-null PV containing the enhanced green fluorescent protein (EGFP) coding sequence with or without $2A^{pro}$ was examined. It expressed fluorescent protein. This result suggests that $2A^{pro}$-deficient PV can express foreign genes.

Poliomyelitis is an acute disease of the central nervous system caused by the poliovirus (PV), a human enterovirus that belongs to the *Picornaviridae* family. Humans are the only natural hosts of PV. In humans, an infection is initiated by oral ingestion of the virus followed by multiplication in the alimentary mucosa (7, 38), from where the virus spreads through the bloodstream. Viremia is considered essential for leading to paralytic poliomyelitis in humans.

PV is a nonenveloped particle that consists of a positive single-stranded RNA genome and 60 copies each of four capsid proteins and occurs in three serologically distinct types, type 1, type 2, and type 3. The genome, composed of approximately 7,500 nucleotides (nt), is polyadenylylated and covalently linked at the 5′ end to a small protein, VPg (31, 40, 44). The RNA alone is infectious; cells transfected with the RNA produce infectious progeny virions. The polyprotein is cotranslationally cleaved by virus-specific proteinases to form viral capsid proteins (VP0, VP1, and VP3) and noncapsid proteins (2A, 2B, 2C, 3A, 3B, 3C, and 3D). VP0 is further cleaved into VP2 and VP4 during the formation of virions. $2A^{pro}$, $3C^{pro}$, and $3CD^{pro}$ are viral proteinases involved in processing specific to PV polyproteins (26). The translation of the viral mRNA is controlled by an internal ribosomal entry site (IRES), a 400-nt RNA segment of the viral genome that precedes the open reading frame (ORF) (33, 34). An IRES element with a similar function exists in the genomic RNA of the encephalomyocarditis virus (EMCV) (19, 20). Molla et al. (29) inserted the type 2 EMCV IRES element into the ORF of PV (at the P1*P2 junction), thereby generating a virus carrying a dicistronic (*dc*) RNA genome. In this *dc* virus, viral proteins are produced by proteolytic processing of two distinct polyproteins, P1 and P2-P3, specifying the capsid proteins and the nonstructural proteins, respectively.

PV defective interfering particles (DIs) have been isolated from laboratory-propagated viral populations (12, 13, 21, 28) and from manipulated cloned infectious cDNAs (16) and, in all cases, retain translational as well as replication competence (28, 32). It has been reported that foreign gene sequences could be substituted into the PV P1 region without affecting the replication of the RNA (4, 37) as long as the translational reading frame was maintained (16). Since the replicons do not encode capsid proteins, they were encapsidated when transfected into cells previously infected with a recombinant vaccinia virus (VV-P1) which expresses the PV capsid precursor, P1 (36). Serial passage of these replicons in the presence of VV-P1 resulted in increasing titers of encapsidated replicons, allowing the generation of stocks of the recombinant PV vectors (36).

In addition to cleaving viral polyproteins, $2A^{pro}$ is known to cleave several cellular proteins. Cleavage of the eukaryotic translation initiation factor eIF4G by $2A^{pro}$ inhibits the cap-dependent translation of cellular mRNA without affecting the translation of viral RNA (15, 24). Independent of the shutoff of

* Corresponding author. Present address: Cancer Stem Cell Project, National Cancer Center Research Institute, 5-1-1 Tsukiji, Chuo-ku, Tokyo, 104-0045, Japan. Phone: 81-3-3547-5201, ext. 4701. Fax: 81-3-3547-5123. E-mail: sohka@ncc.go.jp.

Present address: Institute of Microbial Chemistry, Gotanda, 3-14-23 Kamiosaki, Shinagawa-ku, Tokyo 141-0021, Japan.

▽ Published ahead of print on 14 April 2010.

† The authors have paid a fee to allow immediate free access to this article.

host protein synthesis, $2A^{pro}$ also stimulated the translation of PV RNA (17). The stimulation of translation was later shown to be mediated, at least in part, by the C-terminal cleavage product of eIF4G that is generated by $2A^{pro}$ (8, 18, 45). Therefore, $2A^{pro}$ enhances viral protein synthesis in infected cells both by inhibiting host cell protein synthesis and by stimulating the translation of viral RNA. Several genetic studies suggest $2A^{pro}$ to also have an essential role in PV RNA replication. The replication of a subgenomic RNA replicon which contained a deletion mutation in $2A^{pro}$ was severely inhibited in transfected cells (14). Interestingly, the replication of this RNA could be rescued in *trans* when $2A^{pro}$ was provided by a wild-type helper RNA (14). In addition, studies using a *dc* PV RNA, where the *cis* cleavage function of $2A^{pro}$ was not required to cleave the viral polyprotein, suggested that $2A^{pro}$ activity was essential for efficient viral RNA replication (30). The C-terminal region of $2A^{pro}$ has also been implicated in viral RNA replication (27). $2A^{pro}$ also targets nuclear factors, including several transcription factors (42) and a structural component of small nuclear ribonucleoproteins (snRNPs), gemin-3, which is implicated in the removal of eukaryotic introns mediated by the spliceosome machinery (3). PV $2A^{pro}$ induces alterations in the nuclear pore complex, which inhibits the nuclear export of U snRNA, rRNA, and mRNA but not tRNA. The inhibition of trafficking of *de novo*-synthesized mRNAs occurs early after $2A^{pro}$ expression, suggesting that this protease could prevent host responses to viral infections (11).

PV induces an apoptotic response when its growth is markedly suppressed, for example, in the presence of guanidine hydrochloride. A temperature-sensitive (*ts*) mutant of PV also had suppressed viral growth and induced an apoptotic response. In contrast, a productive infection in these apoptotic cells was accompanied by a canonical necrotic cytopathic effect (CPE) (1, 2, 41). The viral infection triggers an apoptotic pathway involving the consecutive activation of caspase-9 and caspase-3. The productive viral infection suppresses the implementation of this apoptotic program, at least in part, by aberrant processing and degradation of procaspase-9 (6).

Here, we show that a $2A^{pro}$-deficient full-length *dc* PV is replication competent, although the efficiency of its replication is decreased. Moreover, a $2A^{pro}$-deficient P1-null (lacking the entire coding sequence for the capsid proteins) PV with or without enhanced green fluorescent protein (EGFP) can also produce progeny virions under a *trans* supply of P1 protein. Therefore, $2A^{pro}$ is not needed for the replication of PV with or without the P1 coding region in the viral genome, although $2A^{pro}$ plays important roles in PV RNA replication and inducing a CPE.

MATERIALS AND METHODS

Cells, viruses, and antibodies. Monolayers of HeLa and African green monkey kidney (AGMK) cells were grown in Dulbecco's modified Eagle's medium (DMEM; Invitrogen) supplemented with 5% newborn calf serum (NCS; Mitsubishi Kasei), 0.11% $NaHCO_3$ (Wako Pure Chemical Industries Ltd.), and 0.1 mg/ml kanamycin sulfate (Meiji Seika Kaisha, Ltd.) at 37°C under 5% CO_2 and used for the preparation of viruses, transfection with infectious cDNA clones, and plaque assays.

The virulent type 1 PV strain Mahoney [PV1(M)OM], derived from an infectious cDNA clone, pOM1 (39), and the type 3 PV strain Leon were employed in this study. The viruses recovered from the cells transfected with the RNAs of pOMΔ0.8, pOMΔ1.8, pOMΔP1, pOMΔP1Δ2A, pOM-EGFPΔP1, pOM-EGFPΔP1Δ2A, pOME, and pOMEΔ2A were designated OMΔ0.8, OMΔ1.8, OMΔP1, OMΔP1Δ2A, OM-EGFPΔP1, OM-EGFPΔP1Δ2A, OME, and OMEΔ2A, respectively. For providing the PV P1 capsid precursor for P1-defective genomes, a recombinant vaccinia virus (VV-P1) was used (5).

Filtrated ascites fluid of an anti-Mahoney mouse monoclonal antibody (7m008) and an anti-Leon mouse monoclonal antibody (Thai p34-120) were used for the neutralizing assay.

Construction of recombinant cDNAs. pOMΔ0.8 was constructed with a deletion of 816 nucleotides in pOM1 from nucleotide (nt) 1663 to nt 2478 (Fig. 1). Similarly, pOMΔ1.8 had a 1,782-nucleotide deletion in pOM1 from nt 1175 to nt 2956, pOMΔP1 had a 2,628-nucleotide deletion in pOM1 from nt 746 to nt 3373, pOMΔP1Δ2A had a 3,072-nucleotide deletion in pOM1 from nt 746 to nt 3817, and pOMΔP1Δ2AΔ2B had a 3,367-nucleotide deletion in pOM1 from nt 746 to nt 4112. All these plasmids except pOMΔ1.8 were constructed by PCR using KOD Plus DNA polymerase (Toyobo). pOMΔ1.8 was constructed from pOM1 digested by NruI (nt 1172) and SnaBI (nt 2954) and self-ligated.

pOM-EGFPΔP1 was constructed by PCR, subcloning into pBluescript II KS(+), and recombination. Briefly, the fragment from nt 1 to nt 735 of pOM1 which had an XhoI restriction site downstream of nt 735 was digested by KpnI and XhoI and inserted into the equivalent sites of pBluescript II KS(+). This plasmid was designated pBS(1). A fragment amplified from pEGFP-N1 (Clontech) by PCR using a sense primer (MunI>EGFP; 5′-CCCAATTGTATCATA ATGGTGAGCAAGGCG-3′) and an anti-sense primer (EGFP<SmaI; 5′-TCC CCCGGGCTTGTACAGCTCGT-3′) was digested by MunI and SmaI and inserted into the equivalent sites of pBS(1). This plasmid was designated pBS(2). A fragment from nt 3365 to nt 4252 of pOM1 which had a SmaI restriction site just upstream of nt 3365 was digested by SmaI and SpeI (nt 3982 of pOM1) and inserted into the equivalent sites of pBS(2). This plasmid was designated pBS(3). pBS(3) was digested by KpnI and inserted into the equivalent sites of pOM1 (nt 66 and nt 3660). pOM-EGFPΔP1Δ2A was similarly constructed except for the final recombination sites (KpnI [nt 66 of pOM1] and SpeI [nt 3982 of pOM1]).

pOME was constructed by PCR from pOM1 and a plasmid which contains the IRES of EMCV. A fragment containing the PV IRES and P1 coding region with a termination codon which had an EcoRI restriction site just downstream of the termination codon was digested by Bpu1102I (nt 285 of pOM1) and EcoRI (fragment 1). The other fragment contained an EMCV IRES-related region (nt 214 to nt 852 of EMCV cDNA) which had an EcoRI restriction site just upstream of nt 214 of EMCV cDNA and a SmaI restriction site downstream of nt 852 of EMCV cDNA. The sequence of the junction was 5′-(EMCV IRES)-ATG GCC ACA ACC ATG GAA CCC GGG-(SmaI restriction site)-3′. This fragment was digested by EcoRI and SmaI (fragment 2), and fragment 1 and fragment 2 were inserted between the Bpu1102I and SmaI sites of pBluescript II SK(+). This plasmid was designated pBS(4). pBS(4) was digested by Bpu1102I and SmaI (fragment 3). A fragment containing the PV P2-P3 coding region which had a SmaI restriction site just upstream of the sequence required for PV $2A^{pro}$ digestion between PV P1 and $2A^{pro}$ was digested by SmaI and BglII (nt 5601 of pOM1) (fragment 4). The sequence of the junction between the SmaI restriction site and the 2A coding sequence was 5′-(SmaI restriction site) ACC TAC ($2A^{pro}$ coding sequence)-3′. Fragments 3 and 4 were inserted between the Bpu1102I and BglII sites of pOM1, and the final plasmid was designated pOME. pOMEΔ2A was constructed similarly to pOME. The sequence of the junction between the SmaI restriction site and 2B coding sequence was 5′-(SmaI recognition site) GAA GCC ATG GAA CAA (2B coding sequence)-3′.

Nucleotide sequences derived from PCR fragments were analyzed using a BigDye terminator cycle sequencing kit (version 3 or 3.1) (Applied Biosystems) with an ABI Prism 310 genetic analyzer (Applied Biosystems) or ABI Prism 3100-Avant genetic analyzer (Applied Biosystems).

RNA transfection. RNA transcripts were synthesized from PvuI-linearized cDNAs using an AmpliScribe T7 high-yield transcription kit (Epicentre Biotechnologies) and digested with RNase-free DNase I. AGMK cells on a 6-cm dish (Falcon) were transfected with 1 to 3 μg of RNA by a DEAE-dextran method (16). The cultures were harvested at 42 h [for PV1(M)OM and OME] or 75 h (for OMEΔ2A) after the transfection. OMEΔ2A was serially passaged through AGMK cells two times.

Reverse transcription (RT)-PCR. RNA was extracted from PV1(M)OM, OME, OMEΔ2A, OM-EGFPΔP1, and OM-EGFPΔP1Δ2A with chloroform containing phenol and isoamyl alcohol and reverse transcribed with Superscript II transcriptase (Invitrogen) using an anti-sense primer (PV5699<5719 or PV4784<4805). PCR was then performed with KOD Plus (Toyobo) using a sense primer [PV(M)2955>2923] and an anti-sense primer [PV(M)4232<4252] for PV1(M)OM, OME, and OMEΔ2A or using a sense primer (PV577>597) and an anti-sense primer (PV4512<4431) for OM-EGFPΔP1 and OM-EGFPΔP1Δ2A. The PCR products were analyzed by agarose gel electrophoresis.

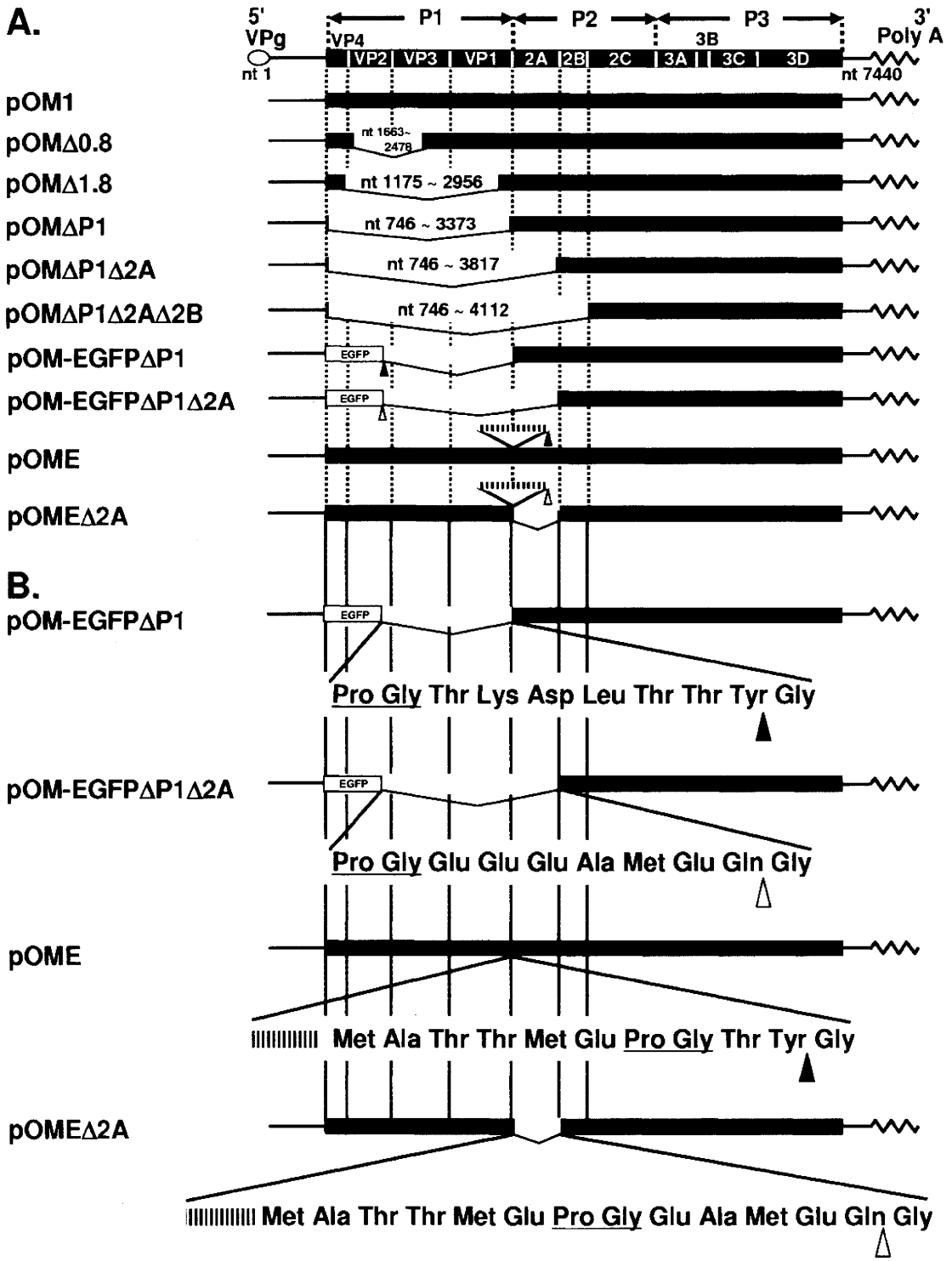

FIG. 1. PV genomic constructions. (A) Construction of PV and recombinant PVs. (B) Junctional amino acid sequences of pOM-EGFPΔP1, pOM-EGFPΔP1Δ2A, pOME, and pOMEΔ2A. The nucleic acid sequence (CCCGGG) recognized by SmaI, corresponding to the amino acid sequence Pro Gly, is shown by underlines. The inserted EMCV IRES are shown by the striped horizontal bars. Closed triangles indicate the sites of cleavage by $2A^{pro}$, and open triangles indicate the sites of cleavage by $3C^{pro}$ or $3CD^{pro}$. Nucleotide numbers of the deleted fragments are shown at the deletion positions.

For sequencing of the products, DNA was extracted from the gels using GenElute Minus ethidium bromide spin columns (Sigma).

Slot blot analysis. Monolayers of HeLa cells (4.4×10^5 cells/well) in 6-well plates were transfected with the *in vitro*-synthesized RNA from each plasmid by the DEAE-dextran method or infected with the viruses. At the time points indicated below, cytoplasmic RNA was extracted from the transfected cells using Isogen (Nippon Gene Co., Ltd.) dissolved in 40 μl of H_2O. One-fourth was mixed with 30 μl of denaturation buffer (66% [vol/vol] formamide and 7.8%

[vol/vol] formaldehyde) in 3-(*N*-morpholino)propanesulfonic acid (MOPS) buffer (26 mM MOPS [pH 7.0], 6.5 mM sodium acetate, and 1.3 mM EDTA) and denatured at 65°C for 5 min, followed by chilling on ice. An equal volume of 20× SSC (333 mM NaCl and 333 mM sodium citrate tribasic dehydrate) was added. In each slot of a slot blotting apparatus (Bio-Dot SF; Bio-Rad Laboratories, Inc.), 10 μl of RNA solution was applied, and the RNA was immobilized on a nylon filter (Hybond-N; GE Healthcare UK Ltd.) and cross-linked by a UV cross-linker (UV Stratalinker1800; Stratagene). The filters were hybridized to a labeled cDNA corresponding to nt 1 to nt 742 of the viral RNA (43) or to exon 7 of glycerol-3-phosphate dehydrogenase (GAPDH) mRNA using AlkPhos Direct (GE Healthcare UK Ltd.) according to the manufacturer's instructions. The probes were detected by chemiluminescence using CDP-Star (GE Healthcare UK Ltd.).

Encapsidation of PV replicons, serial passaging, and purification. The encapsidation and serial passaging of PV replicons using VV-P1 have been described previously (5), and basically the same method was adopted here. Briefly, HeLa S3 cells were infected with 5 PFU of VV-P1, which expresses the PV capsid precursor protein P1, per cell. At 2 h postinfection, the cells were transfected by the DEAE-dextran method with *in vitro*-transcribed RNA. The cultures were harvested at 24 h posttransfection by three successive freeze-thaws, sonicated, and clarified by low-speed centrifugation at 14,000 × *g* for 20 min. For serial passage of the encapsidated replicons and generation of virus stocks, HeLa S3 cells were first infected with 10 to 20 PFU of VV-P1 per cell. At 2 h postinfection, the cells were infected with passage 1 encapsidated replicons. The cultures were harvested at 16 h after PV infection by three successive freeze-thaws, sonicated, and clarified by low-speed centrifugation at 14,000 × *g* for 20 min. The supernatant was then stored at −80°C or used immediately for additional passages by the same procedure.

For purifying the P1-null PV particles, the supernatant was lysed with 1% sodium dodecyl sulfate and centrifuged in a Beckman type 45 rotor at 35,000 rpm for 2.5 h. The supernatant was discarded, and the pellet was washed under the same conditions in 0.1 M phosphate buffer (pH 7.35) for an additional 2.5 h. The pellet was then resuspended in serum-free DMEM, filtrated, and stored at −80°C.

Titration of viruses. The numbers of PFU in AGMK cells were determined by the plaque assay, and the numbers of infectious units (IU) were determined by counting fluorescence-positive cells. Units of viral RNA (U) were adopted for the infection with P1-null viruses. For the measurement of PFU, AGMK cells on 6-cm dishes were inoculated with the viral suspension and then incubated at 37°C for 2 to 5 days for the observation of plaques. To measure the units of viral RNA of OMΔ0.8, OMΔ1.8, OMΔP1, and OMΔP1Δ2A, viral RNA was extracted from the suspensions with chloroform containing phenol and isoamyl alcohol. The units were measured using a LightCycler system (Roche Diagnostics) according to the manufacturer's instructions. As 1.1×10^8 U/ml was equivalent to 2.1×10^9 PFU/ml for PV1(M)OM, we adopted 5.2×10^1 U/cell, which was supposed to be equivalent to 1,000 PFU/cell (multiplicity of infection [MOI] of 1,000) of PV1(M)OM for the infection with OMΔ0.8, OMΔ1.8, OMΔP1, and OMΔP1Δ2A. For the measurement of IU of OM-EGFPΔP1 and OM-EGFPΔP1Δ2A, fluorescence-positive cells were counted under an inverted fluorescence microscope (DM6000B; Leica Microsystems) at 24 h postinfection in HeLa cells. The amount of virus leading to one fluorescence-positive cell was defined as 1 IU. Comparing the units of RNA with the infectious units of fluorescence-positive cells, 5.3×10^9 U/ml was equivalent to 7.1×10^9 IU/ml for an OM-EGFPΔP1 stock and 4.2×10^9 U/ml was equivalent to 1.1×10^9 IU/ml for an OM-EGFPΔP1Δ2A stock. Based on the data, we considered that the units of RNA were not significantly different from the infectious units for OM-EGFPΔP1 and OM-EGFPΔP1Δ2A.

Observation of CPE. HeLa S3 cells in 16-well Lab-Tek chamber slides (Nalge Nunc International K.K.) were infected with PVs. Eight, 18, or 24 h after the incubation with PVs at 37°C, the cells were observed under an inverted microscope.

Neutralization assay. The viral suspension (50 μl) was mixed with filtrated ascites fluid (50 μl) containing the antibody and incubated at 37°C for 1 h. The virus-antibody mixture was overlaid on HeLa S3 cells in 16-well chamber slides and incubated at room temperature for 20 min and then at 37°C for 30 min. The mixture was then replaced with DMEM supplemented with 5% NCS. The cells were observed 18 h after the incubation at 37°C under an inverted microscope.

TUNEL assay. A direct terminal deoxynucleotidyltransferase-mediated dUTP-biotin nick end labeling (TUNEL) assay was performed using an *in situ* cell death detection kit (Roche Diagnostics), and cells were observed under a confocal laser scanning microscope (LSM510; Carl Zeiss MicroImaging Co. Ltd.). Actinomycin D (10 μg/ml) was added for an apoptosis-positive control.

RESULTS

$2A^{pro}$ is not required for full-length *dc* PV to form progeny virus. $2A^{pro}$ is known to be cytotoxic, and a $2A^{pro}$-deficient PV vector might be desirable. To examine whether $2A^{pro}$ is needed to form progeny virus, cDNAs of the full-length *dc* pOME and pOMEΔ2A with the backbone of the PV type 1 Mahoney strain (pOM1) (Fig. 1A and B) were constructed and the ability to form progeny viruses was examined. HeLa cells were transfected with the RNA of pOM1, pOME, and pOMEΔ2A and examined for a CPE. RNA derived from pOM1, pOME, and pOMEΔ2A was not degraded as assessed by gel electrophoresis (data not shown). All these RNAs induced a CPE that led to cell death, whereas no CPE was observed in the mock-transfected cells (data not shown). The supernatants also induced a CPE in HeLa cells. These results show that pOM1, pOME, and pOMEΔ2A can form progeny viruses, called PV1(M)OM, OME, and OMEΔ2A, respectively. This suggests that $2A^{pro}$ is not essential to form progeny virus for full-length *dc* PV.

To confirm that the OME and OMEΔ2A suspensions do not contain IRES deletion revertants, the sizes of the fragments encompassing VP1 and 2B were examined by PCR (data not shown). The PV1(M)OM, OME, and OMEΔ2A suspensions produced appropriate fragments, that is, 1.3-kb, 1.9-kb, and 1.5-kb fragments, respectively. The sequences of the PCR fragments were analyzed, and they were not mutated (data not shown). These results mean that IRES deletion revertants were not detected in the OME and OMEΔ2A suspensions under the experimental conditions and that it is highly probable that these suspensions do not contain IRES deletion revertants. This suggests that OME and OMEΔ2A can proliferate by themselves.

To ascertain that the CPE was actually induced by PV, a neutralization assay was performed using a monoclonal antibody for the virulent type 1 Mahoney strain (7m008) and a monoclonal antibody for the virulent type 3 Leon strain (Thai p34-120). HeLa cells were infected with PV1(M)OM, OME, OMEΔ2A, or Leon at an MOI of 10 in the presence or absence of 7m008 or Thai p34-120 and examined for a CPE (Fig. 2). In the absence of the antibodies, all the strains induced a CPE. In the presence of 7m008, only Leon caused a CPE. In contrast, in the presence of Thai p34-120, all the strains except Leon had a CPE. These results suggest that PV1(M)OM, OME, and OMEΔ2A are type 1 strains, and the CPE was induced by PV.

To define the characteristics of the viral strains, a plaque assay was performed using AGMK cells (Fig. 3). PV1(M)OM produced large plaques, OME moderate-sized plaques, and OMEΔ2A the smallest plaques. The extremely small plaques of OMEΔ2A may relate to its slow replication rate.

To compare these strains further, HeLa cells were infected at an MOI of 10 and cell morphology was observed 8 or 24 h after the infection (Fig. 4). All the viruses had a CPE (Fig. 4A). No CPE was observed in the mock-infected cells. To quantify the rate of CPE-expressing cells, the percentages of round-shaped cells, detached cells, and cells with membrane blebbing among all cells were analyzed, and the kinetics are shown in Fig. 4B. OMEΔ2A had a lesser CPE than did OME or PV1(M)OM. OME exhibited a similar level of CPE to PV1(M)OM, although OME had slightly slower kinetics than

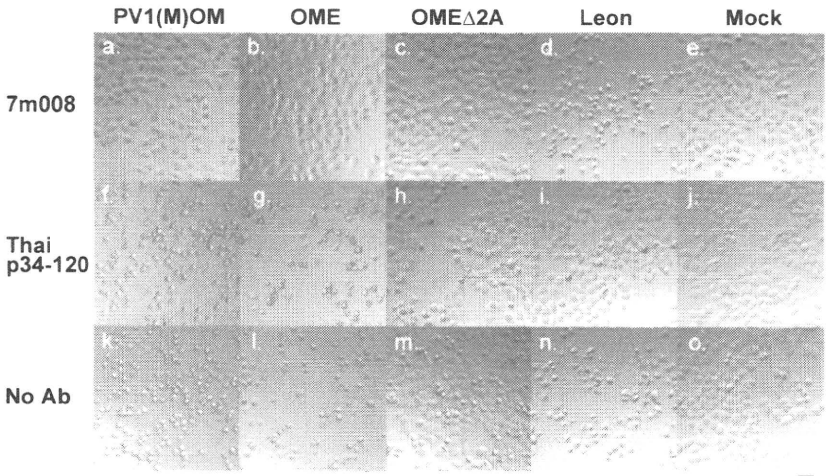

FIG. 2. Neutralization assay of PV1(M)OM, OME, OMEΔ2A, and Leon with anti-PV type 1 or type 2 monoclonal antibody. HeLa cells were mock infected (e, j, and o) or infected with PV1(M)OM (a, f, and k), OME (b, g, and l), OMEΔ2A (c, h, and m), or Leon (d, i, and n) in the absence (k to o) or presence of an anti-PV type 1 Mahoney monoclonal antibody (7m008, a to e) or anti-PV type 2 Leon monoclonal antibody (Thai p34-120, f to j). Eighteen hours after the infection, the CPE was observed under a microscope. Bar, 50 μm.

PV1(M)OM. The results were reproducible. These results suggest that in speed of viral replication and/or the ability to induce CPE, the strains rank as OMEΔ2A < OME ≒ PV1(M)OM. They also suggest that $2A^{pro}$ contributes to efficient viral replication and/or the induction of a CPE. When the cells were infected at a higher MOI (MOI of 50), the kinetics were essentially unchanged (data not shown). This result suggests that an MOI of 10 was high enough to assess the kinetics of CPE expression. Only OMEΔ2A induced morphological changes typical of apoptosis, namely, cell membrane blebbing, in a significant proportion of cells (Fig.4Ac, Ae, and 4Cs). This result indicates that OMEΔ2A may induce apoptosis.

$2A^{pro}$-deficient full-length *dc* PV induces apoptosis. To confirm that OMEΔ2A induces apoptosis, a direct TUNEL assay was performed in cells infected with or without PV1(M)OM or OMEΔ2A or treated with actinomycin D, which induces apoptosis (Fig. 5). Uninfected samples and PV1(M)OM-infected samples contained few fluorescence-positive cells. On the other hand, actinomycin D-treated samples and OMEΔ2A-infected samples included many fluorescence-positive cells. These results suggest that OMEΔ2A induces apoptosis. This raises the possibility that $2A^{pro}$ is important to prevent typical apoptosis in PV-infected cells.

P1-null PV RNA deficient in the $2A^{pro}$ coding region can replicate in cells. It has been reported that the PV P1 coding region is not required for RNA replication and the formation of progeny virus in P1-expressing cells (4, 37). To further define which parts of the PV genome are necessary for RNA replication, deletion mutants were prepared (Fig. 1A) and RNA replication activity was examined by slot blotting (Fig. 6A). RNAs derived from pOM1, pOMΔ0.8, pOMΔ1.8, pOMΔP1, pOMΔP1Δ2A, and pOMΔP1Δ2AΔ2B were not degraded as assessed by gel electrophoresis (data not shown). The RNAs were introduced into HeLa cells, and the cells were collected 2 and 8 h after the transfection. Cell lysates were used for slot blotting. When a probe for PV IRES RNA was used, all the RNAs except for pOMΔP1Δ2AΔ2B RNA were increased at 8 h compared to the levels at 2 h after the transfection. The amounts of GAPDH RNA hardly changed up to 8 h after the transfection. The results were reproducible. These results suggest that the $2A^{pro}$ coding region is not needed for the RNA replication of P1-null PV and that 2B is necessary for the PV replicon activity.

The $2A^{pro}$ coding region is not required for P1-null PV to form progeny virus in P1-expressing cells. Next, the ability to form progeny virus was examined. The RNAs of pOM1,

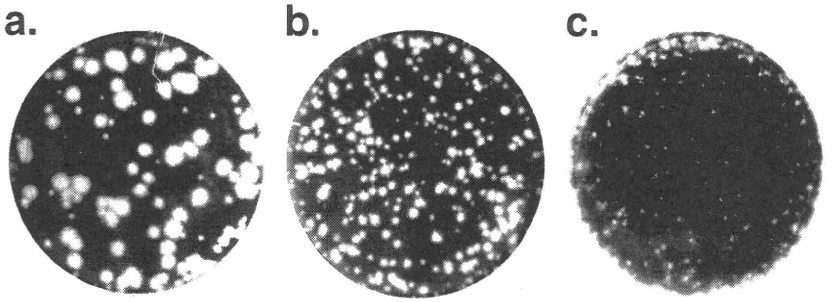

FIG. 3. Plaque phenotypes of PV1(M)OM, OME, and OMEΔ2A. AGMK cells were infected with PV1(M)OM (a), OME (b), and OMEΔ2A (c). The cells were fixed 2 days after the infection with PV1(M)OM, and OME and 4 days after the infection with OMEΔ2A.

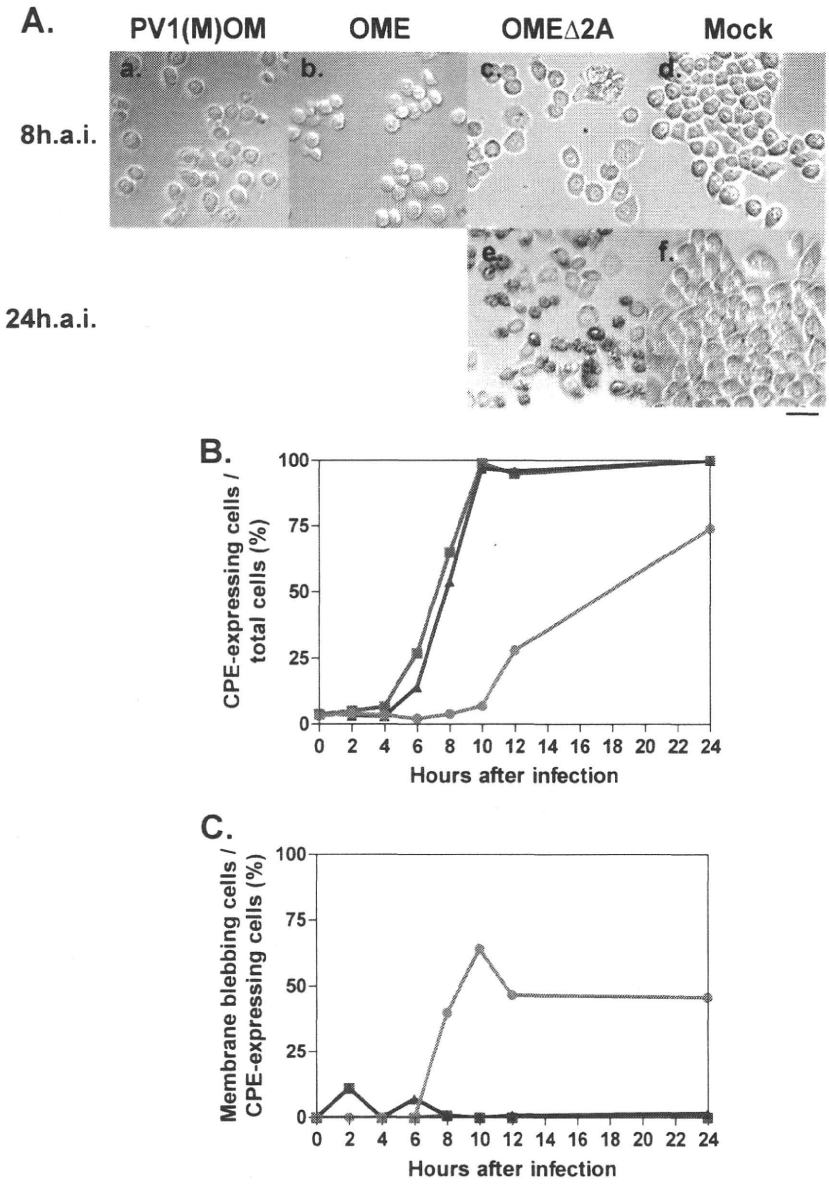

FIG. 4. CPE in cells infected with or without PV1(M)OM, OME, and OMEΔ2A. (A) HeLa cells were mock infected (d and f) or infected with PV1(M)OM (a), OME (b), or OMEΔ2A (c and e) at an MOI of 10. Eight (a to d) or 24 h (e and f) after the infection (h.a.i.), morphological changes were observed under a microscope. Bar, 50 μm. (B) Percentages of CPE expression among all cells. (C) Rates of membrane blebbing among CPE-expressing cells. Average rates in two to three microscopic fields in one experiment were plotted. The rates were examined 0, 2, 4, 6, 8, 10, 12, and 24 h after the infection. Blue lines with squares indicate results for PV1(M)OM, pink lines with triangles indicate results for OME, and orange lines with circles indicate results for OMEΔ2A.

pOMΔ0.8, pOMΔ1.8, pOMΔP1, pOMΔP1Δ2A, and pOMΔP1Δ2AΔ2B were introduced into P1-expressing cells, and the supernatant was recovered after freezing and thawing. HeLa cells were covered with medium containing the supernatants and examined for a CPE 24 h later (data not shown). All the supernatants except those of pOMΔP1Δ2AΔ2B RNA and mock transfectants had a CPE. These results suggest that the RNAs of pOMΔ0.8, pOMΔ1.8, pOMΔP1, and pOMΔP1Δ2A can form progeny viruses, OMΔ0.8, OMΔ1.8, OMΔP1, and OMΔP1Δ2A, respectively, whereas the pOMΔP1Δ2AΔ2B RNA cannot. The quality and sizes of the viral RNA genomes were confirmed by agarose gel electrophoresis (data not shown). To adjust the titers among these viruses, the copy numbers of the PV RNA strands in the virus-containing supernatants were examined by quantitative real-time PCR and the units of viral RNA were determined. To examine the CPE expression, HeLa cells were infected at 5.2×10^1 U/cell and examined for a CPE up to 24 h after the infection (Fig. 7), and the rates of round cells, detached cells, and cells with membrane blebbing among all cells were analyzed (Fig. 7B). Similar to the previous results, all the viruses had a CPE. P1-null PV had slower kinetics than PV1(M)OM. OMΔ0.8, OMΔ1.8, and OMΔP1 showed similar numbers of CPE-expressing cells, although the kinetics of OMΔP1 until 10 h after the infection was faster than that of other P1-null PVs.

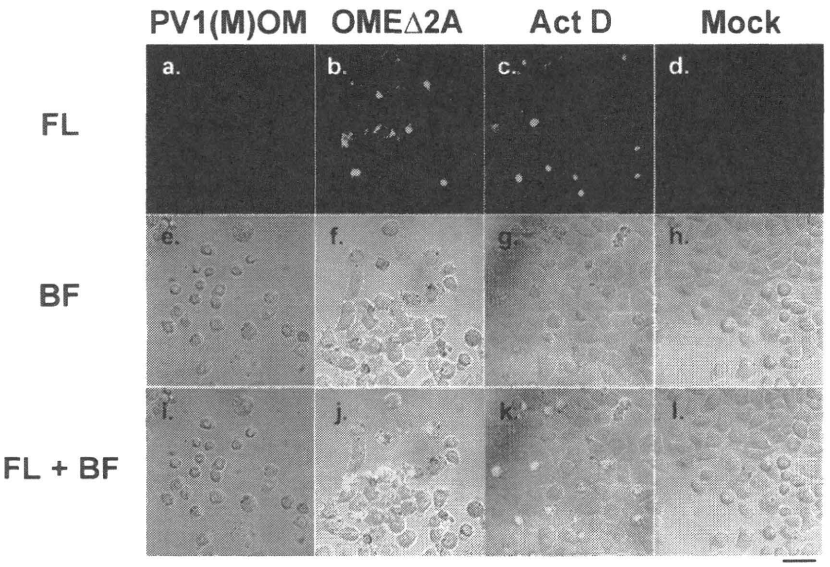

FIG. 5. Apoptosis in cells infected with OMEΔ2A, detected by the TUNEL assay. HeLa cells were mock infected (d, h, and l), infected with PV1(M)OM (a, e, and i) or OMEΔ2A (b, f, and j), or treated without (d, h, and l) or with (c, g, and k) actinomycin D (Act D). Seven hours after the infection with PV1(M)OM, 8 h after the treatment with actinomycin D, and 21 h after the infection with OMEΔ2A, the cells were TUNEL stained. TUNEL-positive cells were fluorescent. Fluorescence (FL) images are shown at the top (a to d), bright-field (BF) images are shown in the middle (e to h), and merged (FL+BF) images are shown at the bottom (i to l). Bar, 50 μm.

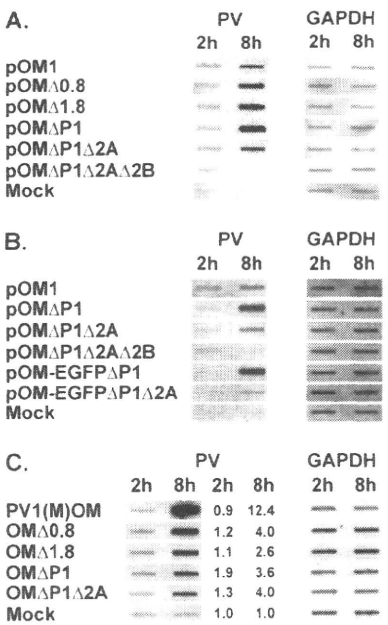

FIG. 6. Slot blot analysis of cells after transfection with or without synthesized viral RNA or after infection with or without viruses. (A) HeLa cells were transfected with or without (Mock) RNAs of pOM1, pOMΔ0.8, pOMΔ1.8, pOMΔP1, pOMΔP1Δ2A, or pOMΔP1Δ2AΔ2B, and cell lysates were collected 2 and 8 h later. The RNAs were detected with probes for the PV IRES sequence or GAPDH sequence. (B) A similar experiment was performed using the RNAs of pOM1, pOMΔP1, pOMΔP1Δ2A, pOMΔP1Δ2AΔ2B, pOM-EGFPΔP1, and pOM-EGFPΔP1Δ2A. (C) HeLa cells were infected with or without (Mock) PV1(M)OM, OMΔ0.8, OMΔ1.8, OMΔP1, or OMΔP1Δ2A, and cell lysates were collected 2 and 8 h later. The RNAs were detected with probes for the PV IRES sequence or GAPDH sequence. Relative amounts of PV RNA corrected to the amount of GAPDH RNA are shown.

OMΔP1Δ2A reproducibly had a lower rate of CPE than other P1-null PVs until 24 h after the infection. This result suggests that OMΔP1Δ2A is less able to induce a CPE or else takes longer and that $2A^{pro}$ plays an important role in inducing a CPE. OMΔP1, significantly, started to cause membrane blebbing typical of apoptosis from 2 h after the infection, and the proportion of CPE-expressing cells was relatively high at early time points (Fig. 7C). This result indicates the possibility that OMΔP1 induces apoptosis. Compared with other P1-null PVs, OMΔP1Δ2A showed at least about a two-times-higher rate of membrane blebbing among CPE-expressing cells at 24 h after infection (OMΔ0.8, 12%; OMΔ1.8, 4.7%; OMΔP1, 7.9%; and OMΔP1Δ2A, 20%) (Fig. 7C). This indicates that OMΔP1Δ2A may induce apoptosis at a relatively low efficiency.

$2A^{pro}$ coding region-deficient P1-null PV vector expresses foreign genes. Because OMΔP1Δ2A can form progeny virus, $2A^{pro}$ may not be essential for P1-null PV to express foreign genes. To examine whether OMΔP1 and OMΔP1Δ2A can express foreign genes, an EGFP coding sequence was inserted into the region of pOMΔP1 and pOMΔP1Δ2A with P1 deleted (Fig. 1A and B). The new constructs were designated pOM-EGFPΔP1 and pOM-EGFPΔP1Δ2A, respectively. RNAs derived from pOM1, pOMΔP1, pOMΔP1Δ2A, pOMΔP1Δ2AΔ2B, pOM-EGFPΔP1, and pOM-EGFPΔP1Δ2A were not degraded as assessed by gel electrophoresis (data not shown). The RNAs were introduced into HeLa cells, and the cells collected 2 and 8 h after the transfection. The cell lysate was used for slot blotting (Fig. 6B). When a probe for PV IRES RNA was used, all the RNAs except for pOMΔP1Δ2AΔ2B RNA increased at 8 h after the transfection compared to the levels at 2 h. pOM-EGFPΔP1 RNA increased more than pOM-EGFPΔP1Δ2A RNA. The amounts of GAPDH RNA hardly changed up to 8 h after the transfection. The results were reproducible. These results suggest that the $2A^{pro}$ coding region is not required for the RNA repli-

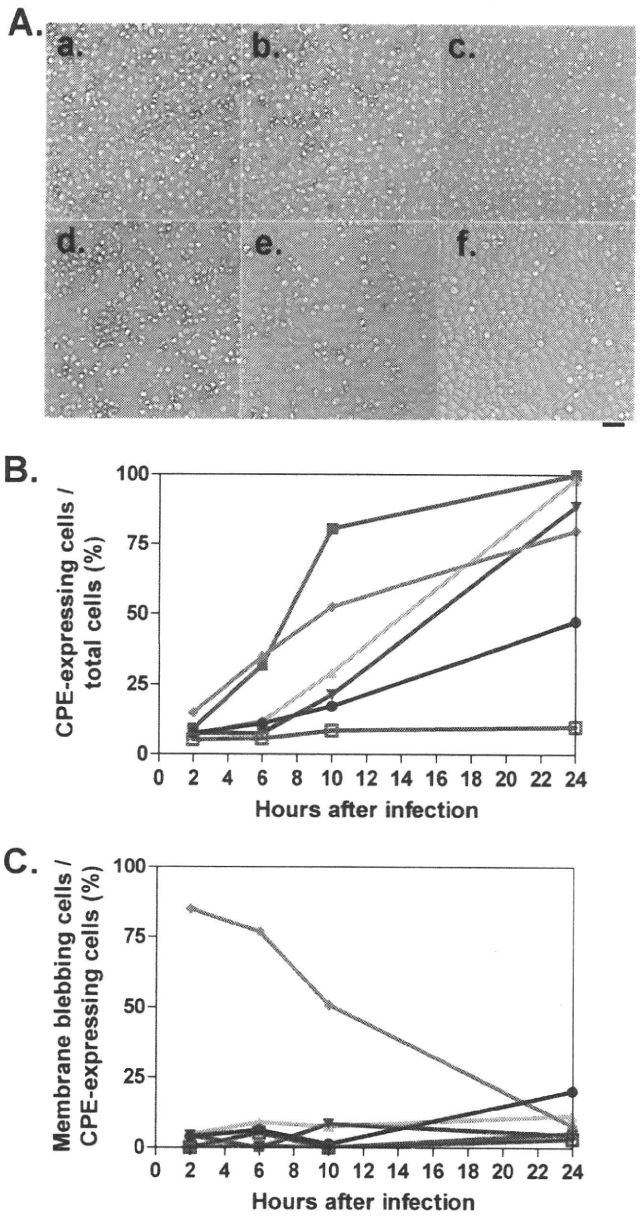

FIG. 7. CPE in the cells infected with PV1(M)OM, OMΔ0.8, OMΔ1.8, OMΔP1, and OMΔP1Δ2A. (A) HeLa cells were mock infected (f) or infected with PV1(M)OM (a), OMΔ0.8 (b), OMΔ1.8 (c), OMΔP1 (d), or OMΔP1Δ2A (e) at an MOI of 1,000, and cell morphology was observed 24 h later under a microscope. Bar, 50 μm. (B) Percentages of CPE expression among all cells. (C) Rates of membrane blebbing among CPE-expressing cells. Average rates in two to four microscopic fields in one experiment were plotted. The rates were examined at 2, 6, 10, and 24 h after the infection. Blue lines with filled squares indicate results for PV1(M)OM, green lines with triangles indicate results for OMΔ0.8, violet lines with inverted triangles indicate results for OMΔ1.8, orange lines with rhombuses indicate results for OMΔP1, pink lines with circles indicate results for OMΔP1Δ2A, and moss-green lines with open squares indicate results for mock-infected cells.

cation of P1-null PV with EGFP inserted, although deletion of the $2A^{pro}$ coding region results in a lower rate of RNA replication. When a probe for PV IRES RNA was used, the RNAs of pOMΔP1 and pOMΔP1Δ2A reproducibly increased to levels similar to the RNAs of pOM-EGFPΔP1 and pOM-EGFPΔP1Δ2A, respectively. These results suggest that the insertion of EGFP does not significantly affect PV RNA replication. Next, the RNAs of pOM-EGFPΔP1 and pOM-EGFPΔP1Δ2A were introduced into P1-expressing cells and the supernatants were recovered after freezing and thawing. The viral particles, OM-EGFPΔP1 and OM-EGFPΔP1Δ2A, respectively, proliferated in P1-expressing cells and were then purified. HeLa cells were covered with the purified virus at an MOI of 100, and the fluorescence of EGFP was observed under the fluorescence microscope 24 h after the infection (Fig. 8). Fluorescence-positive cells were observed in the OM-EGFPΔP1- and OM-EGFPΔP1Δ2A-infected samples, whereas no positive cells were observed in the mock-infected sample. These results suggest that OMΔP1 and OMΔP1Δ2A can express EGFP and that $2A^{pro}$ is not essential for P1-null PV to express EGFP.

In their ability to express EGFP 24 h after the infection, the strains ranked reproducibly as OM-EGFPΔP1Δ2A < OM-EGFPΔP1 (the average rates of fluorescence positivity among all cells in three microscopic fields in one experiment were 23% for OM-EGFPΔP1 and 9.7% for OM-EGFPΔP1Δ2A). This suggests that the defect in $2A^{pro}$ decreases the expression of EGFP and/or the speed of viral replication. OM-EGFPΔP1Δ2A had a CPE, as did OM-EGFPΔP1, but only OM-EGFPΔP1Δ2A reproducibly induced morphological changes typical of apoptosis in a significant proportion of the CPE-expressing cells (the average rates of membrane blebbing among CPE-expressing cells were 10% for OM-EGFPΔP1 and 37% for OM-EGFPΔP1Δ2A). The result implies that $2A^{pro}$ masks apoptosis in a significant proportion of cells. In the speed with which they induced a CPE, the strains reproducibly ranked as OM-EGFPΔP1 ≒ OM-EGFPΔP1Δ2A (the average rates of CPE expression among all cells were 27% for OM-EGFPΔP1 and 26% for OM-EGFPΔP1Δ2A). This suggests that $2A^{pro}$ has little or no effect on inducing a CPE. The quality and sizes of the RNA genomes of OM-EGFPΔP1 and OM-EGFPΔP1Δ2A were confirmed by Northern blotting (data not shown). The genomic stability of OM-EGFPΔP1 and OM-EGFPΔP1Δ2A was examined by general RT-PCR, but no deletion was detected even after 20 passages (data not shown). These results suggest that both OM-EGFPΔP1 and OM-EGFPΔP1Δ2A are genetically stable for at least 20 passages.

DISCUSSION

$2A^{pro}$ has been thought important for PV replication. Here, we reveal that $2A^{pro}$ is not required for PV replication and $2A^{pro}$-deficient PV with or without the capsid coding region can produce progeny viruses. This shows the possibility of realizing a vector that expresses a longer foreign gene and is less toxic.

Molla et al. reported that *dc* PV cDNA without the $2A^{pro}$ coding region (pT7PVE2B) does not produce a viable virus (30). In contrast, RNA of pOMEΔ2A, which has a structure similar to that of pT7PVE2B, resulted in productive although inefficient replication. This may be due to a difference in the junctional sequences between P1 and 2B. In the case of pT7PVE2B, 2B is translated directly from the second EMCV IRES and methionine is added to the N terminus of 2B. On the other hand, in the case of pOMEΔ2A, the additional N-termi-

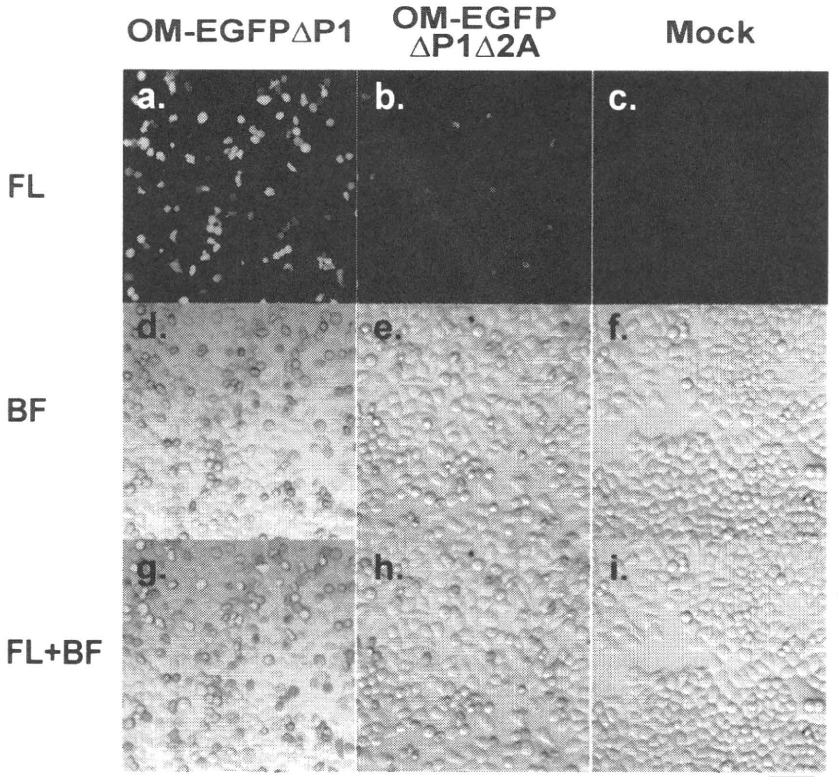

FIG. 8. P1-null PV vector with or without the $2A^{pro}$ coding region expresses EGFP. HeLa cells were mock infected (c, f, and i) or infected with OM-EGFPΔP1 (a, d, and g) or OM-EGFPΔP1Δ2A (b, e, and h) and observed 24 h later under a fluorescence microscope. Upper panels show fluorescence (FL) images (a to c), panels in the middle show bright-field (BF) images (d to f), and lower panels show merged (FL+BF) images (g to i). Bar, 100 μm.

nal sequences of 2B can be processed by $3C^{pro}$ or $3CD^{pro}$. Moreover, pT7PVE2B contains EMCV IRES up to AUG_{834}, whereas pOMEΔ2A contains it up to +18 nt downstream of AUG_{834}. Ribosomal initiation complexes attach directly to AUG_{834}, and initiation does not involve scanning (22, 35). The interaction positions for ribosomal initiation complexes are up to +17 nt downstream of AUG_{834} (23). It is possible that the difference leads to modification of the 2B activity and/or relatively low efficiency of the initiation of the second cistron translation.

OMEΔ2A caused apoptosis, whereas neither PV1(M)OM nor OME did. Our results show the possibility that OMΔP1, OMΔP1Δ2A, and OM-EGFPΔP1Δ2A induce apoptosis in a significant proportion of cells. Calandria et al. reported that independently expressed $2A^{pro}$ and $3C^{pro}$ induced apoptosis by mechanisms involving caspase activation (10). On the other hand, Burgon et al. reported that a 2A N32D mutation independently caused cells to die by apoptosis much earlier than wild-type-infected cells (9). This is consistent with the hypothesis that a wild-type function of the $2A^{pro}$ protein is to inhibit apoptosis and cause a canonical necrotic CPE late in infection, perhaps directly or indirectly leading to the aberrant cleavage of procaspase-9, and that this activity is abrogated by the 2A N32D mutation. Together with our results, it seems likely that the apoptotic cell death induced in the cells infected with 2A-deficient or P1-deficient PV occurs via caspase-dependent apoptosis and that the expression of apoptosis depends on a subtle balance of relating proteins, such as $2A^{pro}$, $3C^{pro}$, and procaspase-9, at each time point after the infection. It is highly possible that the balance of viral proteins differs depending on whether the virus is monocistronic or dicistronic. $2A^{pro}$ activity may differ fundamentally depending on whether this protein is expressed individually or in the context of the viral infection.

It has been reported that PV was replication competent upon the replacement of its P1 region with a foreign gene in P1-expressing cells (4, 37). In these cases, an insert of about 2.9 kilobases (carcinoembryonic antigen [CEA]) was the longest. DIs with a 1,212-base deletion at the longest in the P1 region have been detected (25). We revealed that PV can produce progeny viruses with the entire P1 and $2A^{pro}$ coding region deleted in P1-expressing cells. This construct lacks the longest region. We confirmed that PV can express EGFP without the P1 and $2A^{pro}$ coding regions and that the insertion of EGFP does not significantly affect viral RNA replication. Moreover, these viruses are genetically stable. These results raise the possibility that a longer foreign gene than CEA can be expressed using the PV vector.

OMΔP1Δ2A had a lesser CPE than OMΔ0.8, OMΔ1.8, OMΔP1, and PV1(M)OM at 5.2×10^1 U/cell, which was supposed to be equivalent to an MOI of 1,000 of PV1(M)OM. To correct the units of viral RNA genomes as infectious units, HeLa cells were infected with OMΔ0.8, OMΔ1.8, OMΔP1, and OMΔP1Δ2A at 5.2×10^1 U/cell or with PV1(M)OM at an MOI of 10, the cells were collected 2 and 8 h later, and cell

lysates were used for slot blotting (Fig. 6C). When a probe for PV IRES RNA was used, all the P1-null viruses had increased at almost the same rates at 8 h compared to the levels at 2 h after the infection. PV1(M)OM increased much more than P1-null viruses. These results suggest that 5.2×10^1 U/cell for P1-null viruses results in similar RNA replication activities under these conditions. The viral titers/cell might not be high enough to infect all the cells because the cells infected at 5.2×10^1 U/cell contained more RNA than those infected at 5.2 U/cell (data not shown); it is likely that the units of the RNA genomes of OMΔ0.8, OMΔ1.8, OMΔP1, and OMΔP1Δ2A were almost proportional to these RNA replication activities. Consequently, it was confirmed that OMΔP1Δ2A is less toxic or takes a longer time to have a CPE even though its RNA replication activity is similar to those of OMΔ0.8, OMΔ1.8, and OMΔP1.

Regarding the slot blot analysis of the cells transfected with synthesized viral RNA, the RNAs of pOMΔP1Δ2A and pOM-EGFPΔP1Δ2A showed less RNA replication activity than those of pOMΔP1 and pOM-EGFPΔP1, respectively (Fig. 6B). It seems likely that the defect in $2A^{pro}$ suppresses the RNA replication activity. In terms of the relevant effect of $2A^{pro}$, viral replication speed, and/or the ability to induce a CPE, the ranking was OMEΔ2A < OME and OMΔP1Δ2A < OMΔP1, whereas OM-EGFPΔP1 ≒ OM-EGFPΔP1Δ2A. In the ability to express EGFP, the ranking was OM-EGFPΔP1Δ2A < OM-EGFPΔP1. These results may be also because the defect in $2A^{pro}$ suppresses the viral replication activity and/or the expression of foreign mRNA.

ACKNOWLEDGMENTS

We are grateful to T. Matano, N. Kamoshita, A. Yanagiya, and N. Matsuda for suggestions and discussions. We also thank A. Ohmura for technical support and E. Suzuki for help in preparing the manuscript. We are grateful to C. D. Morrow for generously providing VV-P1.

This work was supported in part by Grants-in-Aid for Advanced Medical Science Research by Ministry of Education, Culture, Sports, Science and Technology (MEXT), a Grant-in-Aid for Scientific Research on Priority Areas, a Grant-in-Aid for Scientific Research (S), a Grant-in-Aid for Scientific Research on Priority Areas, a Grant-in-Aid for Young Scientists (B), a Health Labor Sciences Research Grant, special coordination funds for promoting Science and Technology, contracted research allowance "Research and Development in a New Converting Field Based on Nanotechnology and Materials Science" by MEXT, and The Naito Foundation.

REFERENCES

1. **Agol, V. I., G. A. Belov, K. Bienz, D. Egger, M. S. Kolesnikova, N. T. Raikhlin, L. I. Romanova, E. A. Smirnova, and E. A. Tolskaya.** 1998. Two types of death of poliovirus-infected cells: caspase involvement in the apoptosis but not cytopathic effect. Virology **252:**343–353.
2. **Agol, V. I., G. A. Belov, K. Bienz, D. Egger, M. S. Kolesnikova, L. I. Romanova, L. V. Sladkova, and E. A. Tolskaya.** 2000. Competing death programs in poliovirus-infected cells: commitment switch in the middle of the infectious cycle. J. Virol. **74:**5534–5541.
3. **Almstead, L. L., and P. Sarnow.** 2007. Inhibition of U snRNP assembly by a virus-encoded proteinase. Genes Dev. **21:**1086–1097.
4. **Ansardi, D. C., Z. Moldoveanu, D. C. Porter, D. E. Walker, R. M. Conry, A. F. LoBuglio, S. McPherson, and C. D. Morrow.** 1994. Characterization of poliovirus replicons encoding carcinoembryonic antigen. Cancer Res. **54:** 6359–6364.
5. **Ansardi, D. C., D. C. Porter, and C. D. Morrow.** 1993. Complementation of a poliovirus defective genome by a recombinant vaccinia virus which provides poliovirus P1 capsid precursor in trans. J. Virol. **67:**3684–3690.
6. **Belov, G. A., L. I. Romanova, E. A. Tolskaya, M. S. Kolesnikova, Y. A. Lazebnik, and V. I. Agol.** 2003. The major apoptotic pathway activated and suppressed by poliovirus. J. Virol. **77:**45–56.
7. **Bodian, D.** 1955. Emerging concept of poliomyelitis infection. Science **122:** 105–108.
8. **Borman, A. M., R. Kirchweger, E. Ziegler, R. E. Rhoads, T. Skern, and K. M. Kean.** 1997. eIF4G and its proteolytic cleavage products: effect on initiation of protein synthesis from capped, uncapped, and IRES-containing mRNAs. RNA **3:**186–196.
9. **Burgon, T. B., J. A. Jenkins, S. B. Deitz, J. F. Spagnolo, and K. Kirkegaard.** 2009. Bypass suppression of small-plaque phenotypes by a mutation in poliovirus 2A that enhances apoptosis. J. Virol. **83:**10129–10139.
10. **Calandria, C., A. Irurzun, A. Barco, and L. Carrasco.** 2004. Individual expression of poliovirus 2Apro and 3Cpro induces activation of caspase-3 and PARP cleavage in HeLa cells. Virus Res. **104:**39–49.
11. **Castello, A., J. M. Izquierdo, E. Welnowska, and L. Carrasco.** 2009. RNA nuclear export is blocked by poliovirus 2A protease and is concomitant with nucleoporin cleavage. J. Cell Sci. **122:**3799–3809.
12. **Cole, C. N.** 1975. Defective interfering (di) particles of poliovirus. Prog. Med. Virol. **20:**180–207.
13. **Cole, C. N., D. Smoler, E. Wimmer, and D. Baltimore.** 1971. Defective interfering particles of poliovirus. I. Isolation and physical properties. J. Virol. **7:**478–485.
14. **Collis, P. S., B. J. O'Donnell, D. J. Barton, J. A. Rogers, and J. B. Flanegan.** 1992. Replication of poliovirus RNA and subgenomic RNA transcripts in transfected cells. J. Virol. **66:**6480–6488.
15. **Etchison, D., S. C. Milburn, I. Edery, N. Sonenberg, and J. W. Hershey.** 1982. Inhibition of HeLa cell protein synthesis following poliovirus infection correlates with the proteolysis of a 220,000-dalton polypeptide associated with eucaryotic initiation factor 3 and a cap binding protein complex. J. Biol. Chem. **257:**14806–14810.
16. **Hagino-Yamagishi, K., and A. Nomoto.** 1989. In vitro construction of poliovirus defective interfering particles. J. Virol. **63:**5386–5392.
17. **Hambidge, S. J., and P. Sarnow.** 1992. Translational enhancement of the poliovirus 5′ noncoding region mediated by virus-encoded polypeptide 2A. Proc. Natl. Acad. Sci. U. S. A. **89:**10272–10276.
18. **Hunt, S. L., T. Skern, H. D. Liebig, E. Kuechler, and R. J. Jackson.** 1999. Rhinovirus 2A proteinase mediated stimulation of rhinovirus RNA translation is additive to the stimulation effected by cellular RNA binding proteins. Virus Res. **62:**119–128.
19. **Jang, S. K., M. V. Davies, R. J. Kaufman, and E. Wimmer.** 1989. Initiation of protein synthesis by internal entry of ribosomes into the 5′ nontranslated region of encephalomyocarditis virus RNA in vivo. J. Virol. **63:**1651–1660.
20. **Jang, S. K., H. G. Krausslich, M. J. Nicklin, G. M. Duke, A. C. Palmenberg, and E. Wimmer.** 1988. A segment of the 5′ nontranslated region of encephalomyocarditis virus RNA directs internal entry of ribosomes during in vitro translation. J. Virol. **62:**2636–2643.
21. **Kajigaya, S., H. Arakawa, S. Kuge, T. Koi, N. Imura, and A. Nomoto.** 1985. Isolation and characterization of defective-interfering particles of poliovirus Sabin 1 strain. Virology **142:**307–316.
22. **Kaminski, A., M. T. Howell, and R. J. Jackson.** 1990. Initiation of encephalomyocarditis virus RNA translation: the authentic initiation site is not selected by a scanning mechanism. EMBO J. **9:**3753–3759.
23. **Kolupaeva, V. G., I. B. Lomakin, T. V. Pestova, and C. U. Hellen.** 2003. Eukaryotic initiation factors 4G and 4A mediate conformational changes downstream of the initiation codon of the encephalomyocarditis virus internal ribosomal entry site. Mol. Cell. Biol. **23:**687–698.
24. **Kuechler, E., J. Seipelt, H. D. Liebig, and W. Sommergruber.** 2002. Picornavirus proteinase-mediated shutoff of host cell translation: direct cleavage of a cellular initiation factor, p. 301–311. *In* B. L. Semler and E. Wimmer (ed.), Molecular biology of picornaviruses. ASM Press, Washington, DC.
25. **Kuge, S., I. Saito, and A. Nomoto.** 1986. Primary structure of poliovirus defective-interfering particle genomes and possible generation mechanisms of the particles. J. Mol. Biol. **192:**473–487.
26. **Lawson, M. A., and B. L. Semler.** 1990. Picornavirus protein processing—enzymes, substrates, and genetic regulation. Curr. Top. Microbiol. Immunol. **161:**49–87.
27. **Li, X., H. H. Lu, S. Mueller, and E. Wimmer.** 2001. The C-terminal residues of poliovirus proteinase 2A(pro) are critical for viral RNA replication but not for cis- or trans-proteolytic cleavage. J. Gen. Virol. **82:**397–408.
28. **Lundquist, R. E., M. Sullivan, and J. V. Maizel, Jr.** 1979. Characterization of a new isolate of poliovirus defective interfering particles. Cell **18:**759–769.
29. **Molla, A., S. K. Jang, A. V. Paul, Q. Reuer, and E. Wimmer.** 1992. Cardioviral internal ribosomal entry site is functional in a genetically engineered dicistronic poliovirus. Nature **356:**255–257.
30. **Molla, A., A. V. Paul, M. Schmid, S. K. Jang, and E. Wimmer.** 1993. Studies on dicistronic polioviruses implicate viral proteinase $2A^{pro}$ in RNA replication. Virology **196:**739–747.
31. **Nomoto, A., B. Detjen, R. Pozzatti, and E. Wimmer.** 1977. The location of the polio genome protein in viral RNAs and its implication for RNA synthesis. Nature **268:**208–213.
32. **Omata, T., H. Horie, S. Kuge, N. Imura, and A. Nomoto.** 1986. Mapping and sequencing of RNAs without recourse to molecular cloning: application to RNAs of the Sabin 1 strain of poliovirus and its defective interfering particles. J. Biochem. **99:**207–217.

33. **Pelletier, J., and N. Sonenberg.** 1989. Internal binding of eucaryotic ribosomes on poliovirus RNA: translation in HeLa cell extracts. J. Virol. **63**:441–444.
34. **Pelletier, J., and N. Sonenberg.** 1988. Internal initiation of translation of eukaryotic mRNA directed by a sequence derived from poliovirus RNA. Nature **334**:320–325.
35. **Pestova, T. V., C. U. Hellen, and I. N. Shatsky.** 1996. Canonical eukaryotic initiation factors determine initiation of translation by internal ribosomal entry. Mol. Cell. Biol. **16**:6859–6869.
36. **Porter, D. C., D. C. Ansardi, W. S. Choi, and C. D. Morrow.** 1993. Encapsidation of genetically engineered poliovirus minireplicons which express human immunodeficiency virus type 1 Gag and Pol proteins upon infection. J. Virol. **67**:3712–3719.
37. **Porter, D. C., L. R. Melsen, R. W. Compans, and C. D. Morrow.** 1996. Release of virus-like particles from cells infected with poliovirus replicons which express human immunodeficiency virus type 1 Gag. J. Virol. **70**:2643–2649.
38. **Sabin, A. B.** 1956. Pathogenesis of poliomyelitis: reappraisal in the light of new data. Science **123**:1151–1157.
39. **Shiroki, K., T. Ishii, T. Aoki, M. Kobashi, S. Ohka, and A. Nomoto.** 1995. A new cis-acting element for RNA replication within the 5′ noncoding region of poliovirus type 1 RNA. J. Virol. **69**:6825–6832.
40. **Tobin, G. J., D. C. Young, and J. B. Flanegan.** 1989. Self-catalyzed linkage of poliovirus terminal protein VPg to poliovirus RNA. Cell **59**:511–519.
41. **Tolskaya, E. A., L. I. Romanova, M. S. Kolesnikova, T. A. Ivannikova, E. A. Smirnova, N. T. Raikhlin, and V. I. Agol.** 1995. Apoptosis-inducing and apoptosis-preventing functions of poliovirus. J. Virol. **69**:1181–1189.
42. **Weidman, M. K., R. Sharma, S. Raychaudhuri, P. Kundu, W. Tsai, and A. Dasgupta.** 2003. The interaction of cytoplasmic RNA viruses with the nucleus. Virus Res. **95**:75–85.
43. **Yanagiya, A., Q. Jia, S. Ohka, H. Horie, and A. Nomoto.** 2005. Blockade of the poliovirus-induced cytopathic effect in neural cells by monoclonal antibody against poliovirus or the human poliovirus receptor. J. Virol. **79**:1523–1532.
44. **Yogo, Y., and E. Wimmer.** 1972. Polyadenylic acid at the 3′-terminus of poliovirus RNA. Proc. Natl. Acad. Sci. U. S. A. **69**:1877–1882.
45. **Ziegler, E., A. M. Borman, F. G. Deliat, H. D. Liebig, D. Jugovic, K. M. Kean, T. Skern, and E. Kuechler.** 1995. Picornavirus 2A proteinase-mediated stimulation of internal initiation of translation is dependent on enzymatic activity and the cleavage products of cellular proteins. Virology **213**:549–557.

The Picornaviruses
Edited by Ellie Ehrenfeld, Esteban Domingo, and Raymond P. Roos

Chapter 21

Poliomyelitis

SATOSHI KOIKE AND AKIO NOMOTO

INTRODUCTION

Poliovirus (PV) is the causative agent of poliomyelitis, an acute human disease of the central nervous system (CNS). PV pathogenesis was initially studied in nonhuman primates, beginning soon after the virus was isolated by Landsteiner and Popper (62). General outlines of the sequential events in PV infection were delineated by Bodian, Sabin, and others in the 1950s (6, 8, 106; recently reviewed in references 73, 76, 85, and 99) (Fig. 1).

In humans, PV is ingested and multiplies in the oropharyngeal and intestinal mucosa. Infected humans shed virus in pharyngeal secretions and feces for several weeks, allowing for transmission of the virus. The virus spreads to the draining lymph nodes, where it replicates further, and then spreads via the efferent lymphatic vessels and thoracic duct to enter the bloodstream. Viremia is established, resulting in exposure of almost all tissues to virus. PV replication occurs in extraneural tissues such as spleen, liver, pancreas, muscle, and adipose tissue; however, the amount of recovered virus is low and prominent pathological lesions are not observed in these tissues. Viremia continues for approximately a week, until neutralizing antibodies appear in the blood. Most natural infections of humans end at this stage with a minor illness, such as fever, sore throat, and intestinal upset, a course commonly followed with other enterovirus infections.

In less than 1% of individuals infected with wild-type (wt) PV, the virus spreads to the CNS, where it replicates efficiently. Therefore, neurological disease caused by PV is considered an accidental phenomenon accompanying the common enteric infection. PV replicates in restricted sites of the CNS, including motor neurons in the spinal cord (which leads to flaccid paralysis), the brain stem, and cortex.

Since the development of effective PV vaccines (104, 105, 107), studies on PV pathogenesis using nonhuman primate models have become less common. In 1990, the development of a transgenic (tg) mouse model provided new approaches for the study of PV infection (57, 102). The tg model has provided an opportunity to study the reasons that PV fails to reach the final target tissues in most cases of infection. This failure suggests that there are barriers that prevent the progression and dissemination of PV infection and that neurological disease only occurs when virus succeeds in traveling across the barriers. One may consider that each step of PV infection is a combat between the virus and a host barrier. The nature of some of these barriers has been clarified using the tg mouse model. This chapter will provide a review of recent advances in our understanding of PV pathogenicity from this perspective.

SPECIES SPECIFICITY OF PV INFECTION: THE HOST RANGE BARRIER

PV Receptor and Host Range

The host range of most PV strains is restricted to primates (reviewed in reference 40), with humans as the natural host. Old World monkeys are susceptible to experimental infection, while the susceptibility of New World monkeys is irregular and only some species are susceptible to only some PV strains. Prosimians and nonprimate species are generally not susceptible to PV except for adapted PV strains (2). This host range restriction is determined by the ability of virus to bind to a cell surface receptor, the PV receptor (PVR) (45).

The PVR was identified by taking advantage of the species-specific nature of infection. Mouse cells are not susceptible to PV infection but permit PV

Satoshi Koike • Neurovirology Project, Tokyo Metropolitan Institute of Medical Science, Tokyo Metropolitan Organization for Medical Research, 2-1-6 Kamikitazawa, Setagaya-ku, Tokyo 156-8506, Japan. **Akio Nomoto** • Institute of Microbial Chemistry, 3-14-23 Kamiosaki, Shinagawa-ku, Tokyo 141-0021, Japan.

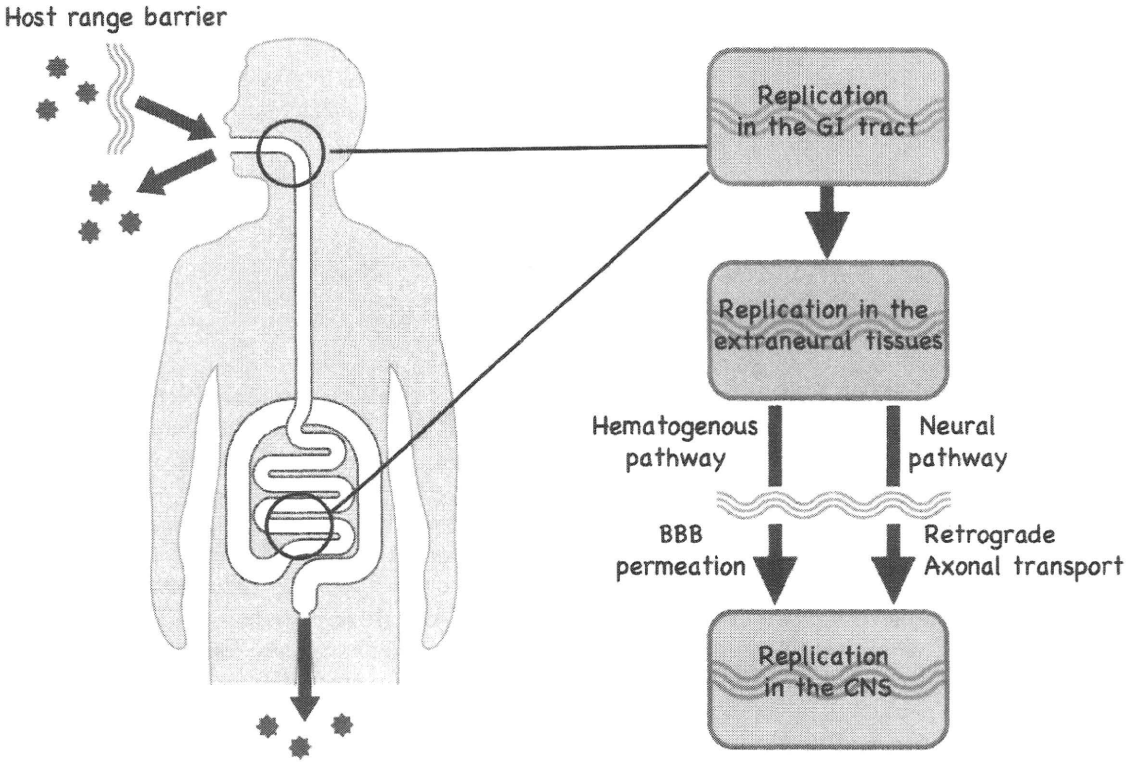

Figure 1. Scheme of PV pathogenesis and possible barriers that prevent PV dissemination. There are several host barriers that block the progression of PV dissemination. The host range of PV is restricted to simians, so other animal species are not susceptible to PV infection (host range barrier). In humans, after PV is ingested, PV initially replicates in the oropharyngeal and intestinal mucosa and enters the host despite a physical barrier at the GI mucosa (GI tract barriers). When PV reaches the blood, PV replicates poorly in the extraneural tissues, suggesting the presence of a barrier that prevents efficient replication of PV in these tissues. The CNS is physically isolated from the extraneural tissues by the blood-brain barrier (BBB), which acts as a physical barrier preventing free movement of substances between the bloodstream and the parenchyma of the CNS. PV permeates this barrier by an unknown mechanism. PV also reaches the CNS via retrograde axonal transport, a pathway for PV that is dependent on the PVR. PV finally replicates in neurons in the CNS. The replication sites in the CNS are restricted to certain neurons, suggesting the presence of unknown barriers in nonsusceptible neurons. Replication of attenuated PV strains is strongly suppressed in neurons, suggesting PV strain-specific barriers in the CNS.

replication when PV RNA is transfected, circumventing infection through the cell surface (36–38). Miller et al. (69) found that human-mouse hybrid cells carrying human chromosome 19 were susceptible to PV. A monoclonal antibody directed against the cell surface of HeLa cells, D171, was able to block PV infection (80). D171 also bound to hybrid cells carrying human chromosome 19. In order to identify the PV receptor, Mendelsohn et al. (67) transformed mouse cells that were not susceptible to PV to susceptible cells through the transfer of human genomic DNA. The *PVR* gene was then identified by isolating the human gene responsible for this transforming activity (53, 68). PVR, later designated CD155, is an integral transmembrane protein that has three immunoglobulin (Ig)-like domains and is encoded on chromosome 19.

The interaction between PV and PVR has been extensively investigated. The N-terminal Ig-like domain of PVR is responsible for PV binding (23, 54, 108). This domain penetrates the "canyon" that surrounds the five-fold protrusion on the capsid surface. The binding site involves all three major capsid proteins, VP1, VP2, and VP3. There are several critical amino acid residues in PVR for binding that have been identified by both mutational analyses (1, 4, 70) and cryo-electron microscopy (3, 33). Amino acid sequences of CD155 have been found to rapidly change during evolution. Of note, the critical amino acids in CD155 are not conserved in orthologs of nonsusceptible animal species (45, 50, 55).

Development of tg Animal Models

Soon after the isolation of the human *PVR* gene, attempts were made to generate tg mice, anticipating that the expression of human PVR would make nonsusceptible mice susceptible. Indeed, tg mice that

express the human *PVR* gene with its natural promoter are susceptible to PV infection (56, 57, 102). The infected mice exhibit clinical signs and pathological lesions that resemble human poliomyelitis after intracerebral, intraperitoneal, intravenous, intramuscular, or intranasal inoculation of PV (15, 56, 57, 75, 101, 102). Unlike humans, however, these tg mice are not susceptible to oral infection.

Despite the inability to orally infect tg mice, the development of mouse models has improved investigations of PV dissemination in an animal. In addition to monkeys, PVR-Tg21 mice are recognized by the World Health Organization as an animal model of poliomyelitis (19). tg mice have also been generated in which PVR is expressed under the control of artificial promoters, including cPVR mice with the β-actin promoter (15), fatty acid-binding protein (FABP)–PVR mice with the rat FABP promoter (118), and CAG-PVR mice with the CAG promoter (43). The tg mice have also made it possible to investigate the importance of host genes with respect to the pathogenesis of PV infections by crossing the tg mice with mice in which genes of interest have been modified.

PV REPLICATION IN THE GI TRACT: THE GI BARRIER

Site of Entry and Primary Multiplication

PV enters into the systemic circulation after ingestion of the virus. There are a number of structures that are important in understanding PV infection by the oral route. The majority of the epithelial cells lining the gastrointestinal (GI) tract form a tight barrier that is the first physical barrier for PV infection. A structure called the follicle-associated epithelium (FAE) is located in Peyer's patches above the lymphoid follicle and contains microfold (M) cells, which are capable of transporting molecules from the intestinal lumen into the underlying lymphoid cells (79, 90) (Fig. 2). The mechanism by which PV invades the lymphoid tissues is still unknown.

In humans, chimpanzees, and cynomolgus monkeys, which are susceptible to oral PV infection, a significant titer of PV initially appears in lymphatic tissues, such as the tonsils in the pharynx and Peyer's patches in the small intestine (9, 112); however,

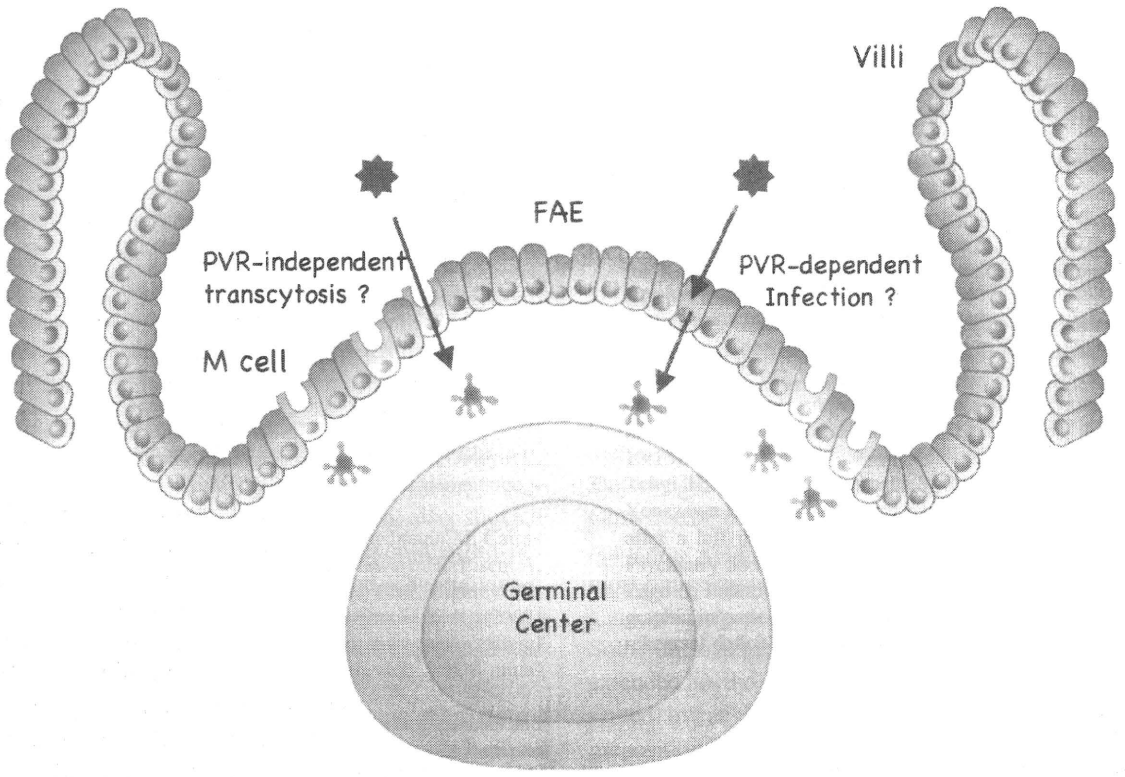

Figure 2. Structure of the GI tract barrier. The epithelial cells (enterocytes) lining the GI tract form a tight physical barrier for PV infection. A structure called FAE is present in Peyer's patches above the lymphoid follicle and contains M cells, which are capable of transporting molecules from the intestinal lumen into the underlying dendritic cells or macrophages. The primary replication sites of PV and the source of excreted virus have not yet been determined. It is also unknown whether PV replicates in the epithelial cells in a PVR-dependent manner or whether PV is incorporated via M cells by transcytosis without lytic infection.

specific histopathological lesions are not clearly correlated with these presumed sites of multiplication (8). Rhesus monkeys (39) and PVR tg mice are not susceptible by this route of infection (57, 102). Some researchers have conducted experiments to elucidate the mechanism by which PV enters the systemic circulation by comparing susceptible and nonsusceptible species; however, the experiments performed have generally been incomplete and with inconsistent results (see below) (46, 47, 89, 109, 110, 118). Therefore, it is still not known which types of cells are infected and how PV accesses lymphatic tissues.

One idea proposed is that PV invades epithelial cells and lymphatic tissues by a direct infection that depends on the expression of PVR. Kanamitsu et al. (47) infected cynomolgus monkeys with the Mahoney strain and, by using immunofluorescence analysis, observed viral replication in squamous epithelial cells and macrophages in the lymphatic structure of the tonsils. This result suggested that the entry of PV into lymphatic tissues is associated with replication in these cells. Iwasaki et al. (46) compared the sites of PVR expression in humans, rhesus monkeys, and PVR tg (PVR-Tg21) mice. They observed PVR expression in epithelia, including the FAE and M cells of Peyer's patches and the germinal center of the follicle in humans. In rhesus monkeys, however, PVR expression was low, while in PVR-tg mice, PVR was barely observable in epithelium and absent in germinal centers. Those authors hypothesized that PVR expression in these sites is important in establishing PV infection in the GI tract. These findings have not been confirmed by experiments involving PV infection. Zhang and Racaniello (118) considered that the resistance of PVR tg mice to oral injection was due to the absence of PVR expression in cells that are critical to support PV replication in this region. These investigators generated a new tg mouse that expressed PVR under the rat FABP promoter in order to test whether enhanced PVR expression in the epithelial cells would result in susceptibility to oral infection. The FABP-PVR mice did not become susceptible to oral infection; however, a detailed analysis of the Peyer's patch cells of the FABP-PVR mice and the expression of PVR were not reported, so it remains unclear whether PVR expression in this tissue is necessary for the establishment of oral infection.

Other reports support the entry of PV by transcytosis through M cells, as is the case with other pathogens. Electron microscopic analysis by Sicinski et al. (109) showed that PV adhered to the surface of M cells and vesicles and that PV was incorporated in the M cells on the FAE. In another report, Ouzilou et al. (89) cultured Caco-2 cells in the upper chamber of a transwell with freshly prepared lymphocytes in the lower chamber. The Caco-2 cells formed a layer sealed with tight junctions. Some cells in the layer differentiated into M-like cells, serving as an in vitro model of FAE. When PV was added to the upper chamber, intact PV was recovered within 2 h from the lower chamber, suggesting that PV can pass through the Caco-2 layer by transcytosis in M cells.

PV REPLICATION IN EXTRANEURAL TISSUES: THE INNATE IMMUNE BARRIER

Roles of PVR and IRES *trans*-Activating Factors

PV replicates in extraneural tissues during the viremic phase. In addition, PV can be recovered from extraneural tissues of orally infected chimpanzees and cynomolgus monkeys (9, 112) and from tg mice infected intravenously (44, 52); however, the amounts of PV recovered are relatively small. No pathological changes are discernible in these tissues. The results suggest that the extraneural tissues are not fully permissive to PV infection, in contrast to the extensive replication that occurs in the CNS. The reason for the extensive replication of PV in the CNS has not been elucidated. One possible hypothesis is that factors that support PV replication are expressed preferentially in the target tissues. Holland proposed that PVR is the determinant of PV tissue tropism (36); however, PVR expression is observed in a wider range of tissues, including resistant ones, suggesting that PVR is necessary but not the sole determinant of PV tropism (22, 57, 58, 68, 100).

It is known that the internal ribosome entry site (IRES) in the 5′ noncoding region (5′ NCR) can function in a tissue- and cell-type-specific manner. Pilipenko et al. (96) demonstrated that a chimeric Theiler's murine encephalomyelitis virus in which the 5′ NCR IRES was replaced by the corresponding region of foot-and-mouth disease virus (FMDV) was not able to replicate in the CNS. The FMDV IRES required a noncanonical translation initiation factor, IRES *trans*-activating factor 45, which is expressed in proliferating cells. This finding suggested that the tissue-specific replication ability of FMDV is controlled by a tissue-specific IRES activity that is mediated by a *trans*-acting factor with tissue-specific expression. Similarly, Gromeier et al. (27) and Yanagiya et al. (115) produced chimeric viruses between human rhinovirus and PV and between hepatitis C virus and PV, respectively. These chimeras lost the ability to replicate in the CNS, suggesting that the IRES of human

rhinovirus and hepatitis C virus is controlled in a tissue-specific manner and does not work in the CNS. However, Kauder and Racaniello (48) produced a recombinant adenovirus that had a bicistronic reporter with the PV IRES in the second cistron. The PV IRES mediated translation not only in the neural tissues but also in extraneural tissues. Thus, it is not likely that the PV IRES mediates preferential replication of PV in the CNS. As we will discuss later, the PV IRES has an important role in replication efficiency in the CNS.

Role of Interferon Response in Tissue Tropism

Ida-Hosonuma et al. (44) reported that a transient increase in PV titer was found in extraneural tissues of infected PVR tg mice. This finding prompted the investigators to speculate that the cells in extraneural tissues are also susceptible to PV and can initiate the replication process but that progression of the infection cascade was inhibited by an unknown mechanism. The reason for the inability of virus to efficiently replicate in extraneural tissues was clarified by experiments using mice deficient in the type I interferon (IFN) response. The results showed that PVR tg mice that were IFN-α/β receptor 1 (IFN-α/βR1) deficient (74) were highly susceptible to PV infection. Interestingly, in the absence of the normal IFN response, PV was able to replicate efficiently not only in the CNS but also in extraneural tissues, such as liver, spleen, and pancreas. The results suggested that extraneural tissues possess all the host factors required for PV replication but that an active host innate immune defense prevents viral replication in these sites. Of note, extraneural tissues express a higher basal activity of IFN-stimulated genes, even in the noninfected state, than neural tissues. In addition, the IFN response induced in response to PV infection in extraneural tissues is greater than in neural tissues.

This difference in the type I IFN response in the two tissues may be the reason for the differences in replication efficiency of PV. Furthermore, Ohka et al. (83) observed that PV replication in the small intestine was enhanced in IFN-α/βR1-deficient PVR tg mice. These results suggested that the IFN response can also act as a barrier to prevent PV replication in extraneural tissues (Fig. 3), constituting an innate immune barrier rather than a physical barrier. The

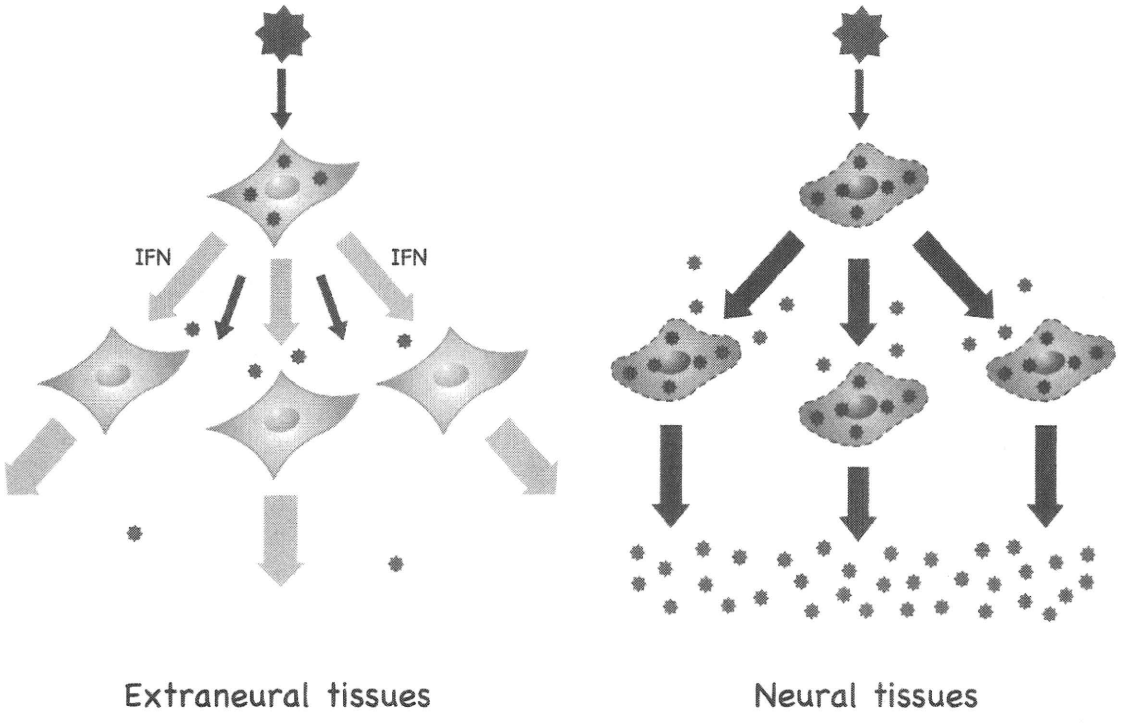

Figure 3. Innate immune barrier in extraneural tissues. Although many tissues are exposed to PV during the viremic phase, PV replication in the extraneural tissues is strongly suppressed by the innate immune response, which is mediated by type I IFN. Many cells in the extraneural tissues possess all of the host factors required for PV replication and have the potential to support PV replication. Soon after infection of a single cell, an active host innate immune defense induces an antiviral state in the surrounding cells and stops the cascade of viral infection in these sites. Thus, this response acts as an immunological barrier. In neural tissues, however, the innate immune response is less active than in the extraneural tissues, allowing a sequential cascade of viral infection.

barrier controls the permissiveness of extraneural tissues and keeps the levels of viremia low. This barrier may be the reason that PV invasion into the CNS occurs in less than 1% of infections, even in nonimmune individuals. In contrast, a relatively weak IFN response in the CNS permits PV replication once the virus reaches the CNS. Thus, the IFN response, which does not function equally in all tissues, is an important factor that determines the neurotropic nature of PV. The importance of the IFN response in protection of nontarget tissues has also been described for other virus infections (24, 71, 103, 113).

CNS ENTRY OF PV: HEMATOGENOUS AND NEURAL PATHWAYS

The CNS is isolated from the extraneural tissues. To date, at least two pathways by which PV invades the CNS are known: via the blood-brain barrier (BBB) and by retrograde axonal transport.

Penetration of the BBB

The BBB, which is composed of endothelial cells of blood vessels that are sealed together at their edges by tight junctions, does not allow free transport of materials, including pathogens, between the bloodstream and parenchyma of the CNS (25). Therefore, the BBB acts as a physical barrier to PV dissemination (Fig. 4); however, PV is believed to invade the CNS through the BBB.

Coyne et al. (14) showed that cultured human brain microvascular endothelial cells, which serve as an in vitro model of the BBB, are susceptible to PV infection. In addition, human endothelial cells from the umbilical vein become susceptible to PV after cultivation in vitro (13). These data, however, do not directly prove that endothelial cells are susceptible to in vivo PV infection, since it is known that cells derived from nonsusceptible tissues can acquire PV susceptibility to infection after cultivation in vitro (20, 117). Data from in vivo studies actually suggest that the invasion of the BBB by PV does not involve infection of endothelial cells. Yang et al. (116) performed a physiological pharmacokinetic analysis to investigate the fate of PV inoculated into the tail vein of mice. The inoculated virus was distributed to various tissues, such as the spleen, liver, kidney, small intestine, heart, lung, muscle, and CNS tissues. The amount of PV delivered to the CNS tissues was significantly greater than the theoretical amount estimated within the vascular volume. In contrast, the amount of PV distributed to other tissues almost equaled the theoretical amount predicted based on vascular volume. These data suggested that PV passes into the parenchyma of the CNS through the BBB. Of interest, the distribution profiles of the virus in tg and non-tg mice were similar, indicating that PVR expression in tg mice (and therefore infection of endothelial cells) does not play a significant role in the tissue distribution profile of PV. The rates of accumulation of the virus in the brain are more than 100 times higher than that of albumin (which is not thought to permeate the BBB via a specific transport system) and are similar to that of cationized rat serum albumin (which is known to efficiently permeate the BBB). The above data suggest that PV penetrates the BBB with a fairly high degree of efficiency, independent of expression of the PVR. Thus, it is possible that host cell molecules other than PVR are involved in the penetration of the BBB by PV. The precise mechanism by which PV entry into the CNS occurs remains to be elucidated.

Retrograde Axonal Transport

Another pathway leading to neural dissemination of PV is by means of retrograde axonal transport, which has been reported for humans, monkeys, and tg mice (Fig. 4). This pathway first drew attention during the Cutter vaccine incident (78), in which children received incompletely inactivated polio vaccine prepared from virulent PV strains; it was observed at that time that the initial paralysis was frequently seen in the inoculated limb. In addition, experimental evidence indicates that PV can spread to the CNS through the sciatic nerve of monkeys (77) and tg mice (101). Of note, there is also a correlation between muscle trauma during the viremic phase of PV infection and an increased risk of poliomyelitis (10), suggesting that the neural pathway is important in this phenomenon of "provocation poliomyelitis." Provocation poliomyelitis was experimentally reproduced in tg mice (28), with results that suggested that skeletal muscle injury stimulates retrograde axonal transport of PV and thereby facilitates viral invasion of the CNS, with resultant spinal cord damage. These findings renewed interest in studying the mechanism by which PV uses neural pathways to enter the CNS.

Mechanism of Axonal Transport of PV

Experiments involving transection of the sciatic nerve following intramuscular inoculation of PV into the calf of PVR tg mice demonstrated that some of the inoculated virus moves along the axon via retrograde

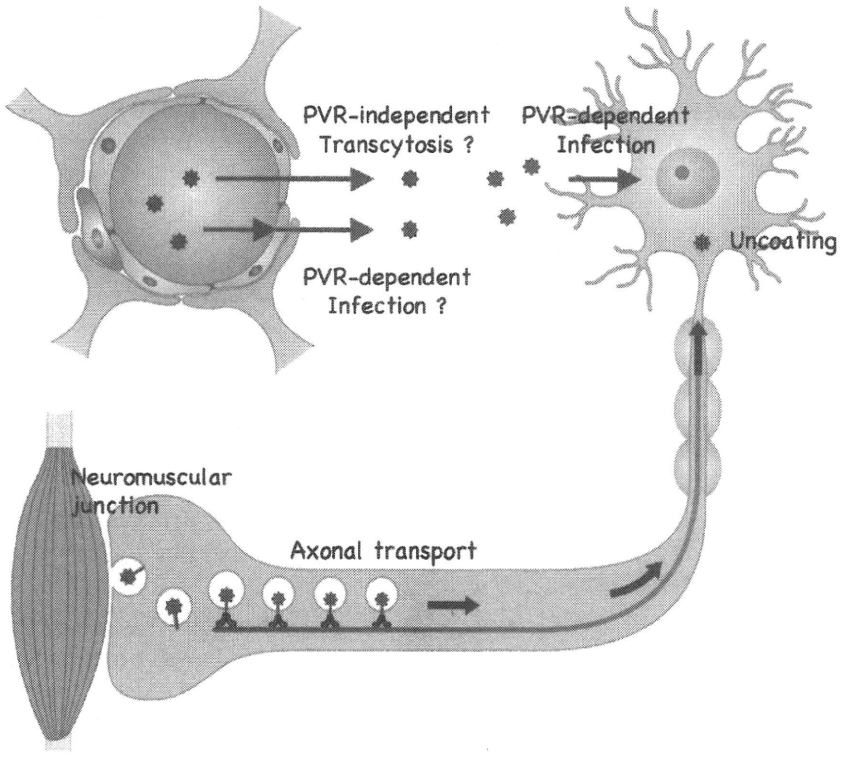

Figure 4. Two pathways of CNS invasion. PV is able to enter the CNS by at least two distinct pathways. One pathway involves the direct penetration of the BBB from the bloodstream into the parenchyma of the CNS. The BBB is composed of endothelial cells of blood vessels that are sealed together at their edges by tight junctions. Generally, it does not allow free transport of pathogens. There is no strong evidence that supports direct infection of endothelial cells. Physiological pharmacokinetic analysis suggests that the PV is able to permeate the BBB from the bloodstream into the parenchyma of the CNS independently of PVR. The precise mechanism by which PV employs this pathway remains to be elucidated. Another pathway leading to neural dissemination of PV is by retrograde axonal transport. PV is incorporated into endosomes by PVR-mediated endocytosis at neuromuscular junctions. The C-terminal cytoplasmic tail of the PVR on the surface of the endosome is able to bind TCTEL1 (in humans) or Tctex-1(in mice), which is the light chain-1 of the cytoplasmic dynein complex. PV-containing endosomes move on the microtubules along the axon via retrograde transport at a rate of more than 12 cm/day, a velocity classified as fast retrograde axonal transport. PV particles do not initiate conformational changes during transport along the axon until they reach the cell body of the neuron.

transport at a rate of more than 12 cm/day (87), a velocity seen with fast retrograde axonal transport (12). These results suggested that PV is packed in endosomes during transport through the axon, since this is the case with many substances that are carried via retrograde transport by the fast transport system. Indeed, an electron microscopic study detected endosomes containing PV at the neuromuscular junction in the vicinity of the inoculation site. Thus, it is possible that PV is within endosomes that result from PVR-mediated endocytosis of the virus at synapses and are then conveyed via retrograde transport through the axon (84).

The majority of PV-related materials in the sciatic nerve showed a sedimentation coefficient of 160S, suggesting that the PV is conveyed without conformational change in the axon and initiates the uncoating step after reaching the cell body of the neurons (87). Of interest, a human homolog (TCTEL1) of mouse Tctex-1, which is the light chain-1 of the cytoplasmic dynein complex (a complex that uses microtubules as pathways for transport), has been reported to bind the cytoplasmic domain of PVR (72, 84). In addition, treatment of the sciatic nerve with the microtubule-depolymerizing agent vinblastine results in slower retrograde transport of the virus to the spinal cord of tg mice (84). It is possible that PV inoculated intramuscularly is incorporated into cells by PVR-mediated endocytosis at synapses, without any PVR-mediated conformational changes of the virion particle. The cytoplasmic domain of PVR on the surface of the endosomes that enclosed the poliovirion could then interact with cytoplasmic dynein, and the endosomes could be retrograde transported

along microtubules through the axon to the neuron cell body, where uncoating and replication of PV occur. A reconstituted experimental system with rat primary neurons was established in order to test the above hypothesis. Molecular imaging experiments indicated that endosomes carrying both PV and PVR undergo retrograde transport through the axons of the primary neurons (86); however, additional research is required to elucidate the mechanisms underlying the endocytosis of PV at synapses and the manner and location of PV replication in the neuron cell body.

PV REPLICATION IN THE CNS

Determinants of Neuron-Specific Infection

In the CNS, PV preferentially infects motor neurons in the anterior horn of the spinal cord and in neurons in the brain stem and motor cortex (7, 11). PV infection is not observed in other sites, including the occipital lobe of the cerebral cortex. Lytic replication of PV in the motor neurons results in a characteristic flaccid paralysis of the limbs. Similar pathology is observed in PVR tg mice. Neuron-specific infection in the CNS seems to be determined by the presence of PVR, because in situ hybridization experiments demonstrated that PVR mRNA expression is observed in neurons but not in glial cells in mice that express PVR with the natural PVR promoter (56, 100); PV infection is observed in glial cells when PVR is expressed in glial cells under the control of a ubiquitous promoter in mice (43). On the other hand, it remains unclear why PV preferentially infects a subset of neurons. Bodian hypothesized that the route of infection, the neuronal network connections, and the intrinsic resistance of some neurons to infection determine this specificity (7, 11).

Role of the IRES in Attenuation of Neurovirulence

Wild-type PV strains replicate more efficiently and produce more severe pathological lesions in the CNS than attenuated strains. The degree of neurovirulence in different virus strains appears to primarily depend on the ability of the virus to replicate in the CNS. There are multiple neurovirulence determinants in the PV genome (60, 88, 114), with strong neurovirulence determinants mapped in the 5′ NCR of all three PV strains. Comparative sequence analysis between the attenuated Sabin 3 strain and its neurovirulent revertants demonstrated that a key mutation at nucleotide position 472 leads to a neurovirulent phenotype (21). Molecular genetic analysis employing reverse genetics of PV type 1 showed that a relatively strong determinant of neurovirulence resides in the 5′ NCR of the viral RNA, especially nucleotide position 480 (49); a neurovirulence determinant in the PV type 2 genome has been identified at nucleotide position 481 (64). These nucleotide positions exist within the region corresponding to the IRES (31, 91). The results suggest that the neurovirulence levels of individual PV strains correspond with their IRES activities, that is, efficient translation initiation in the CNS. It is also known that translation initiation mediated by the IRES of attenuated strains is lower than that of virulent strains in neuroblastoma cell lines (32, 61). Therefore, it is considered that the attenuation phenotype of vaccine strains is due to a neuronal cell-specific translational defect; this translational defect constitutes a barrier specific for attenuated strains.

Possible Mechanism for IRES-Mediated Attenuation In Vivo

Several proteins that interact with the PV IRES have been identified (5, 16, 35, 41, 66, 81, 82, 92). One of these proteins, polypyrimidine tract-binding protein (PTB), has been shown to play an important role in the translational activity of the PV IRES (34, 92). Depletion of PTB from cellular extracts inhibits translation mediated by the PV IRES in a cell-free system (34, 41, 42), and overexpression of PTB in cultured cells enhances translation mediated by the PV IRES (26). Examination of the interaction of PTB with the PV IRES has demonstrated impaired binding by PTB on the Sabin IRES in comparison with the wt IRES (30, 82). Interestingly, CNS cells express PTB at very low levels but contain high levels of a neural or brain-enriched homolog of PTB, nPTB (51, 63, 65, 98).

Guest et al. (29) examined the interaction of the IRESs of PV type 3 virulent Leon strain and Sabin 3 strain with PTB and nPTB. PTB and nPTB were found to bind to a site directly adjacent to the attenuating mutation, and binding at this site was less efficient on the Sabin 3 IRES than on the Leon IRES. The translational activities mediated by the IRES elements of Leon and Sabin 3 were determined by electroporating a bicistronic construct that contained either the Sabin 3 or the Leon 5′ untranslated region into neural cells of a living chicken embryo spinal cord. Translation in the chicken embryo spinal cord mediated by the Sabin 3 IRES was less efficient than translation mediated by the Leon IRES and was rescued by overexpression of PTB, but not nPTB or other IRES *trans*-activating factors. These data suggest that tissue-specific expression of PTB coupled to a reduced binding of PTB on